Geophysical Journal International

Geophys. J. Int. (2025) **241,** 17–34
Advance Access publication 2025 January 17
GJI Seismology

https://doi.org/10.1093/gji/ggaf022

Slow slip events and megathrust coupling changes contribute to the earthquake potential in Oaxaca, Mexico

C. Villafuerte,[1,*] V. M. Cruz-Atienza,[2] J. Tago,[3] D. Solano-Rojas,[3] R. Garza-Girón,[4,†] S. I. Franco,[2] L. A. Dominguez[2] and V. Kostoglodov[2]

[1]*Laboratoire de Géologie, Département de Géosciences, École Normale Supérieure, PSL Université, CNRS UMR, F-8538 Paris, France. E-mail: villafuerte.cd@gmail.com*
[2]*Instituto de Geofísica, Universidad Nacional Autónoma de México,Circuito de la Investigación Científica s/n, C.U., Coyoacán, 04510, Mexico City, Mexico*
[3]*Facultad de Ingeniería, Universidad Nacional Autónoma de México, Circuito Escolar 04360, C.U., Coyoacán, 04510, Mexico City,, Mexico*
[4]*Department of Earth and Planetary Sciences, University of California, Santa Cruz, 95064, USA*

Accepted 2025 January 9. Received 2024 December 16; in original form 2023 September 20

SUMMARY

Stress accumulation on the plate interface of subduction zones is a key parameter that controls the location, timing and rupture characteristics of earthquakes. The diversity of slip processes occurring in the megathrust indicates that stress is highly variable in space and time. Based on global navigation satellite system and interferometric synthetic aperture radar data, we study the evolution of the interplate slip-rate along the Oaxaca subduction zone, Mexico, from October 2016 through October 2020, with particular emphasis on the pre-seismic, coseismic and post-seismic phases associated with the 2020 June 23 M_w 7.4 Huatulco earthquake (also known as La Crucecita earthquake), to understand how different slip regimes contribute to the stress accumulation in the region. Our results show that continuous changes in both the aseismic stress-releasing slip and the coupling produced a high stress concentration [i.e. Coulomb failure stress (CFS) of 80 kPa] prior to the event on the region with the highest moment release of the Huatulco earthquake (between 17 and 30 km depth) and a stress deficit zone in the adjacent updip region (i.e. shallower than 17 km depth with CFS around −90 kPa). This region under negative stress accumulation can be explained by possible recurrent shallow slow slip events (SSE) offshore Huatulco as well as by the stress shadow from adjacent locked segments. Absent in the literature, the shallow rupture is characterized by a secondary slip patch (between 7 and 14 km depth) that overlaps with the highest concentration of aftershocks. Two months prior to the event, a M_w 6.6 long-term SSE also occurred about 80 km northwest from the hypocentre, between 25 and 55 km depth. Transient increments of the interplate coupling around the adjacent 1978 (M_w 7.8) Puerto Escondido rupture zone correlate with the occurrence of the last three SSEs in Oaxaca far downdip of this zone, possibly associated with along-dip fluid diffusion at the subduction interface. Throughout the 4-yr period analysed, the interface region of the 1978 event experienced a high CFS build up of 80–150 kPa, primarily attributable to both the coseismic and early post-seismic slip of the Huatulco rupture, that, considering the 55 yr average return period of the region, indicates large earthquake potential near Puerto Escondido. Continuous monitoring of the interplate slip-rate thus provides a better estimation of the stress accumulation in seismogenic regions than those given by long-term, time-invariant coupling models and improves our understanding of the megathrust mechanics where future earthquakes are likely to occur.

Key words: Seismic cycle; Earthquake dynamics; Earthquake source observations; Episodic tremor and slip.

*Now at: Instituto de Geofísica, Universidad Nacional Autónoma de México, Mexico City, Mexico.

†Now at: Department of Geosciences, Colorado State University, Fort Collins, CO, USA.

1 INTRODUCTION

Large earthquakes along subduction zones occur in regions known as asperities (Lay & Kanamori 1981), which represent areas of the interplate contact where frictional resistance allows elastic stress to build up during tens to hundreds of years as a consequence of the relative plate motion. Under the simple concept of Coulomb failure criterion, an earthquake occurs when the shear stress overcomes the strength of the fault. Both stressing-rate and fault strength are parameters that vary in time and space during the megathrust earthquake cycle. Therefore, understanding the tectonic and mechanical processes that cause these variations is essential to assess the seismic hazard in subduction zones.

Interseismic coupling maps obtained from geodetic observations have been widely used to identify heterogeneous, highly locked segments of the plate interface where large earthquakes take place (Chlieh *et al.* 2008; Moreno *et al.* 2010; Perfettini *et al.* 2010; Loveless & Meade 2011). Most of these estimations consider a steady-state long-term deformation during interseismic periods that results in a time invariant locking pattern. However, it has been observed that interplate coupling also varies with time (Heki & Mitsui 2013; Melnick *et al.* 2017) and might be caused by different processes such as pore pressure transients (Cruz-Atienza *et al.* 2018; Materna *et al.* 2019; Warren-Smith *et al.* 2019) or dynamic stresses from regional earthquakes (Delorey *et al.* 2015; Materna *et al.* 2019; Cruz-Atienza *et al.* 2021). Additionally, recent studies have used the geodetic information from interseismic periods to directly estimate the strain budget by means of fault-stress mechanical inversions (Xie *et al.* 2019; Saito & Noda 2022, 2023).

During the interseismic period, a broad spectrum of tectonic processes occurs on the plate interface with distinctive spatiotemporal characteristics that play an important role to accommodate the strain along the megathrust. Among these processes, short-term and long-term slow slip events (SSEs), which are aseismic slip transients lasting from days to months, release the strain accumulation in the deeper and shallower segments of the plate interface (Beroza & Ide 2011; Saffer & Wallace 2015). Since their discovery, observations and theoretical models have shown that SSEs increase the stress in the adjacent seismogenic zone and may trigger damaging earthquakes (Segall & Bradley 2012; Obara & Kato 2016; Uchida *et al.* 2016; Voss *et al.* 2018). Moreover, it has been documented that major interplate earthquakes in different subduction zones are preceded by SSEs (Kato *et al.* 2012; Ito *et al.* 2013; Radiguet *et al.* 2016; Socquet *et al.* 2017; Cruz-Atienza *et al.* 2021), although the actual mechanisms of their interaction remain under debate.

In the Mexican subduction zone, the recurrence of M_w 7+ interplate earthquakes is ∼30–50 yr (Singh *et al.* 1981). In the deeper segment of the megathrust (30–50 km depth), long-term SSEs occur in Oaxaca and Guerrero with recurrence time of ∼1.5 and ∼3.5 yr, respectively (Cotte *et al.* 2009; Graham *et al.* 2016). The last five M_w 7+ interplate events in the Guerrero and Oaxaca subduction zone were preceded by SSEs in the downdip adjacent region: The 2014 M_w 7.4 Papanoa earthquake (Radiguet *et al.* 2016) and the 2021 M_w 7.0 Acapulco earthquake in Guerrero and three more in Oaxaca, the 2012 M_w 7.5 Ometepec earthquake (Graham *et al.* 2014a), the 2018 M_w 7.2 Pinotepa earthquake (Cruz-Atienza *et al.* 2021) and, as we will demonstrate here, the 2020 M_w 7.4 Huatulco earthquake. Although SSEs do not always trigger large earthquakes, they do interact periodically with the adjacent locked regions and thus contribute with the total stress built-up of the seismogenic zone.

Three years before the 2020 Huatulco earthquake, a complex sequence of SSEs and devastating earthquakes took place from June 2017 to July 2019 in central and southern Mexico, including the M_w 8.2 Tehuantepec and M_w 7.1 Puebla-Morelos earthquakes in 2017 (Melgar *et al.* 2018; Singh *et al.* 2018; Mirwald *et al.* 2019; Suárez *et al.* 2019), and the M_w 7.2 Pinotepa earthquake in 2018 (Li *et al.* 2020), describing a cascade of events interacting with each other on a regional scale via quasi-static and/or dynamic perturbations (Cruz-Atienza *et al.* 2021). During this sequence, two SSE occurred in Oaxaca, in 2017–2018 (O-SSE1) and 2019 (O-SSE2) with M_w 6.9 (Table 1; Cruz-Atienza *et al.* 2021). These SSEs are located where previos SSEs have been documented in the region (Correa-Mora *et al.* 2008; Graham *et al.* 2016).

Table 1. Dates and magnitudes of all slow slip events in Oaxaca from June 2017 to June 2020, as well as the afterslip of the 2018 M_w 7.2 Pinotepa (PE-afterslip) and 2020 M_w 7.4 Huatulco (HE-afterslip) earthquakes.

Events	Dates	M_w
O-SSE1[a]	01/06/2017–15/02/2018	6.9
PE-Afterslip[a]	16/02/2018–22/11/2018	7.2
O-SSE2[a]	16/02/2018–22/11/2018	6.9
O-SSE3[b]	26/12/2019–23/06/2020	6.6
HE-Afterslip[b]	23/06/2020–22/10/2020	7.3

[a] From Cruz-Atienza *et al.* (2021), [b] This study.

Here we thoroughly study the evolution of the interplate slip-rate history in the Oaxaca segment during this unprecedented sequence. Unlike the prior work of Cruz-Atienza *et al.* (2021), here we have removed seasonal effects in the global navigation satellite system (GNSS) displacement time-series and reinverted the slip history specifically in the region of Oaxaca where we have included the pre-seismic, coseismic and post-seismic phases of the 2020 Huatulco earthquake. Our aim is to understand how the different slip processes contribute to the seismic potential in the region. We first introduce the slip solutions of the coseismic phase of the 2020 Huatulco earthquake, together with the unreported preceding SSE and its afterslip phase. Then, we analyse in detail the complex evolution of the slip-rate along the Oaxaca segment to finally elucidate its role in the stress accumulation in the seismogenic zone and how this is compared with the stress accumulation produced by time invariant coupling models. We show that continuous and simultaneous monitoring of SSEs and the megathrust coupling provides a better estimation of the stress accumulation on the locked regions where future large earthquakes are expected to occur.

2 THE 2020 M_w 7.4 HUATULCO EARTHQUAKE

2.1 Coseismic slip inversion

On 2020 June 23, a shallow M_w 7.4 interplate thrust earthquake took place in the state of Oaxaca, Mexico (Fig. 1), within the aftershock area of the 1965 M_w 7.5 earthquake, the last interplate rupture in this region (Chael & Stewart 1982). The hypocentral coordinates, latitude = 15.822°, longitude = −96.125° and depth = 18.2 km, were determined from regional seismic records including station HUAT of the Mexican National Seismological Service (SSN, its acronym in Spanish), located 7 km south of the epicentre (Fig. 2b). We combined near-field GNSS and interferometric synthetic aperture radar (InSAR) data to determine the coseismic slip distribution by means of ELADIN (elastostatic adjoint inversion), a newly developed adjoint inversion method that honours physically

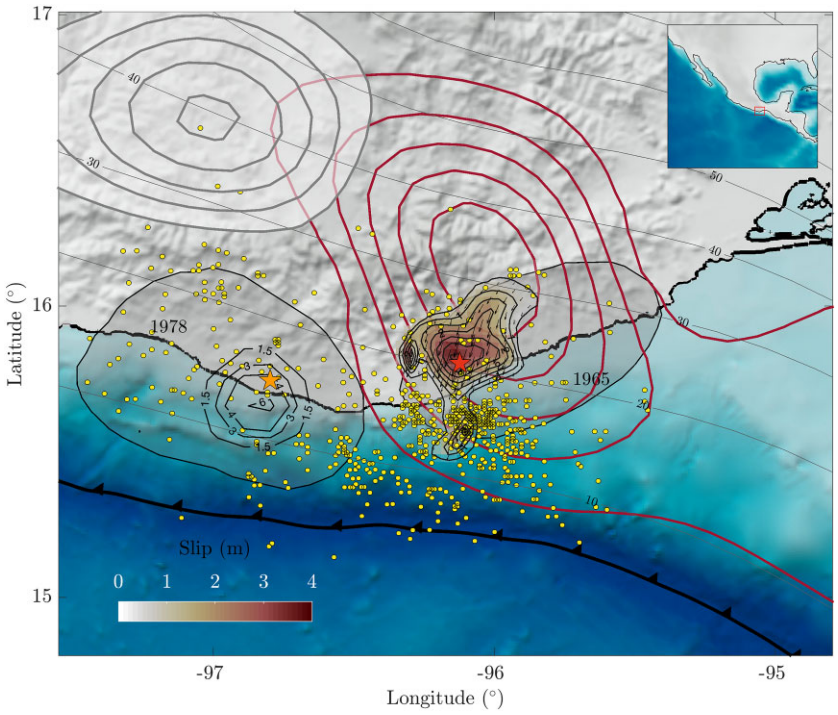

Figure 1. Study region and slip inversions for pre-seismic, coseismic and post-seismic phases of the 2020 M_w 7.4 Huatulco earthquake. Red coloured region with black contours indicates the slip on the plate interface for our preferred joint GNSS and InSAR coseismic slip inversion with slip isolines every 0.5 m beginning with 0.5 m. White shaded patch with grey contours indicate the downdip SSE that took place before the event with slip isolines every 1 cm beginning with 0.5 cm. Red contours depict the afterslip following the Huatulco event with slip isolines every 10 cm beginning with 5.0 cm. Red and orange stars indicate the epicentres of the Huatulco and the 1978 Puerto Escondido earthquakes, respectively. Black contours around the 1978 Puerto Escondido epicentre represent the slip isolines (in m) determined by Mikumo *et al.* (2002). Dark grey shaded patches show the aftershock areas of the historic thrust earthquakes of 1965 Huatulco and 1978 Puerto Escondido. Yellow dots depict the first 50 d Huatulco earthquake aftershocks reported by the SSN. Grey lines parallel to the trench indicate the iso-depths (in km) of the 3-D plate interface used for the slip inversions in this study.

consistent restrictions (e.g. rake angle and von Karman slip distributions) via a gradient projection strategy (Tago *et al.* 2021) (see Supplementary Information).

For the GNSS data (see Supplementary Information for data processing details), we used daily averaged displacements on seven sites with epicentral distance smaller than 160 km. Three-component coseismic discontinuities in all sites were estimated independently from one-day extrapolations of two regression functions before and after the earthquake. Before the earthquake we used linear regressions over 30-d-long windows, while after the earthquake, following Savage *et al.* (2005), we used a logarithmic function of time of the form $A + B \log t$ to fit the data over 45-d-long windows. For both regressions the day of the earthquake was excluded, and their corresponding values extrapolated (yellow dots, Fig. S1, Supplementary Information). Coseismic discontinuities, reported in Fig. S1, Supplementary Information and shown as vectors in Fig. 2(c), are simply the differences of the extrapolated values. At station HUAT, 7 km south of the epicentre, we found a vertical GNSS uplift of 53.2 ± 1.2 cm (Fig. 2c and Fig. S1, Supplementary Information), which is consistent with an independent estimate from a collocated tide gauge recording of 49 ± 5 cm (see Fig. S2, Supplementary Information for data processing details). Seaward horizontal displacement in this site, first reported here, is 41.1 ± 0.6 cm.

For the InSAR data (see Supplementary Information for data processing details), the line-of-sight (LOS) displacement map (Figs 2a and b) was generated from scenes taken before the earthquake, on June 19, and two days after the earthquake, on June 25, by the Sentinel satellite of the *European Space Agency* on ascending track 107, with LOS azimuth at HUAT station of 258.8° and elevation angle of 56.9°. Maximum LOS displacement of 65.3 cm was found about 10 km west from the HUAT.

For the coseismic slip inversion, we assumed a planar fault discretized by 5 x 5 km^2 sub-elements with focal mechanism (strike = 271°, dip = 17° and rake = 70°) determined by the United States Geological Survey (USGS) through the W-phase inversion. To find the optimal data weights for the joint inversion of GNSS and InSAR data, we first inverted each data set individually. Both independent solution models produced an almost perfect data fit but significantly different slip distributions, as shown in Supplementary Information Figs S3b and S3c. Numerous joint inversion tests led us to the optimal data weights (see Supplementary Information) producing a solution that honours the most prominent features of both independent models and satisfactorily explains the whole set of observations, with average GNSS and InSAR data errors of 0.19 ± 0.26 cm and 0.63 ± 0.5 cm, respectively (Fig. 2d and Supplementary Information Fig. S3a).

Following the Mobile Checkerboard (MOC) strategy introduced by Tago *et al.* (2021), we performed resolution tests for the joint GNSS and InSAR inversion considering patch sizes of 21 and 30 km with a von Karman correlation length (L) of 5 km (see Supplementary Information). Our resolution analysis reveals that average restitution indexes (ARI, a metric that minimize the resolution dependence on the checkerboard position) above 0.8 enclose the region where rupture took place (Fig. 3), which means that our preferred slip model (Fig. 2c) has a nominal error below 20 per cent with respect to the actual slip distribution for patches larger than ∼21 km length.

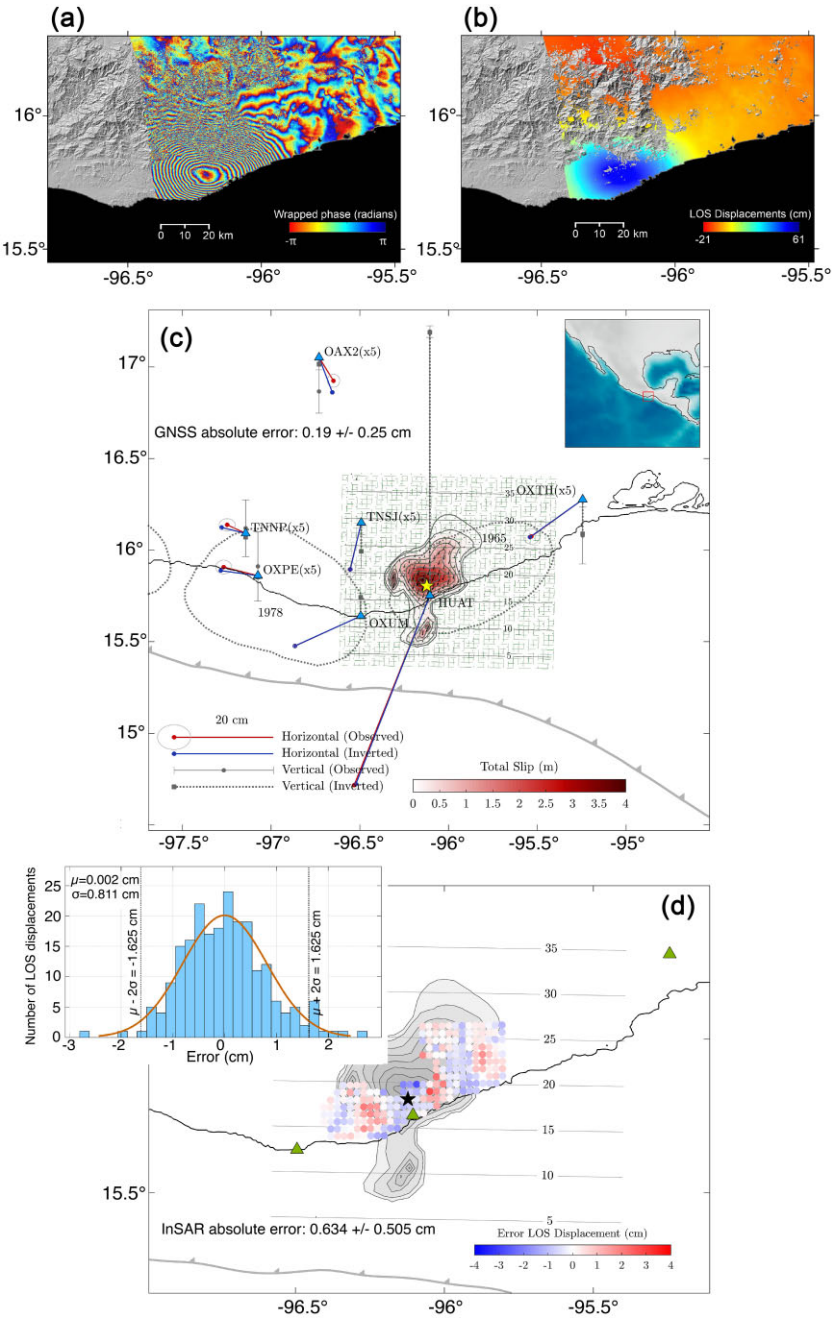

Figure 2. Coseismic slip of the Huatulco earthquake and GNSS and InSAR data used for the inversion. (a) Wrapped phase ascending interferogram estimated from Sentinel satellite images on Track 107 Ascending for scenes on 2020 June 19 and 25. (b) Line-of-sight (LOS) displacement from ascending track, positive values correspond to motion towards the satellite. (c) Joint slip inversion with the observed and predicted displacements in the seven GNSS stations. (d) Misfit between observed and predicted LOS surface displacements for our preferred slip model. The inset figure illustrates that the errors exhibit a normal distribution, with a mean value near zero.

Our preferred slip solution (Fig. 2c) features a prominent slip patch slightly downdip from the hypocentre, between 15 and 25 km depth, with peak slip of 3.6 m and a second, smaller offshore patch 30 km updip from the hypocentre not yet reported in the literature, with an average slip value of 1.5 m. Such prominent coseismic subevent offshore was not reported in previous investigations likely due to the lack of the well-resolved 3-D displacement vector next to the hypocentre at the SSN station HUAT, first used here. Our slip solution shares characteristics with previous slip models that assumed different hypocentral locations and/or focal mechanisms, such as the large downdip slip patch and the main rupture directivity towards the north–northeast, downdip from the hypocentre (Guo *et al.* 2021; Melgar *et al.* 2021; Wen *et al.* 2021; Yan *et al.* 2022). However, unlike all previous solutions, our model explains well both, the uplift and seaward displacements at HUAT, the nearest GNSS station, which is critical to constrain the offshore rupture propagation (Figs 1 and 2c). Three more features stand out from our model: (1) the updip end of the main rupture patch is very close to the nucleation point, (2) the downdip slip limit (33 km depth) might correspond to the end of the locked segment of the

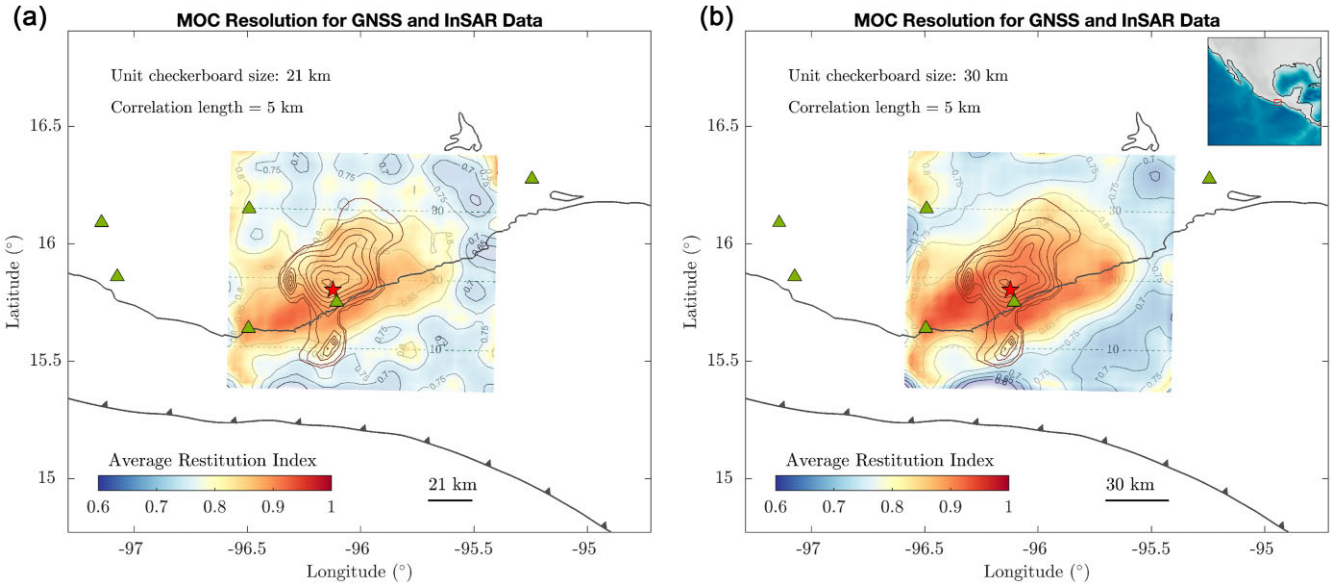

Figure 3. Resolution analysis for the coseismic GNSS+InSAR joint inversion. Average restitution index (ARI) obtained from a mobile checkerboard (MOC) analysis that integrates 64 independent checkerboard inversions with patch sizes of (a) 21 km and (b) 30 km using a correlation length (L) of 5 km. Triangles are the GNSS stations. Grey contours show our preferred slip model for the 2020 Huatulco earthquake and the red star the epicentre.

megathrust, as observed for the 2018 Pinotepa Earthquake (Li *et al.* 2020), the 2012 Ometepec Earthquake (UNAM-Seismology-Group 2013) and the aftershocks areas of regional interplate earthquakes (e.g. the white patch of the 1965 rupture, Fig. 1) and (3) the offshore slip patch is coincident with the highest density of aftershocks (Fig. 1).

2.2 The 2020 Oaxaca SSE that preceded the earthquake

Two months before the Huatulco earthquake, on mid-April 2020, three GNSS stations in Oaxaca (TNNP, TNNX and OAXA) changed their secular interseismic motion from northeast to southwest, indicating a transient deformation associated with a SSE (light blue section in Fig. 4a). We used daily continuous displacement records on 14 permanent GNSS stations in Oaxaca (green triangles in Figs 4b and c) belonging to the SSN and Tlalocnet (Cabral-Cano *et al.* 2018), between September 2019 and the Huatulco earthquake date (Fig. S4, Supplementary Information) to simultaneously invert for the plate interface coupling (PIC, i.e. $1 - v/v_{pl}$, where v is the interplate slip rate, v_{pl} is the plate convergence rate and $v \leq v_{pl}$) and any stress-releasing slip episode (i.e. SSEs) in successive time windows using ELADIN (Figs 4b–e). To this end, we carefully denoised the displacement time-series by fitting and removing harmonic signals with periods of 365 (annual), 365/2 (semi-annual) and 365/3 d related to seasonal effects and periodic GNSS constellation patterns (Amiri-Simkooei *et al.* 2007). Regressions of the harmonic functions were conducted following an inter-SSE multi-window strategy as detailed in the Supplementary Information (Fig. S5). For the aseismic slip inversions, we assumed the 3-D plate interface geometry introduced by Cruz-Atienza *et al.* (2021) and discretized it with subfaults of 10 x 10 km^2. Given both the interface geometry and the distribution of the GNSS stations in Oaxaca, we adopted the optimal von Karman regularization length of 40 km and Hurst exponent of 0.75 used by Tago *et al.* (2021) and Cruz-Atienza *et al.* (2021) to perform a detailed slip resolution analysis following the MOC strategy (see Supplementary Material). Results for three different checkerboard sizes of 100, 70 and 50 km length are summarized in Supplementary Information Fig. S6 (bottom row), from which we conclude that slip solutions between 5 and 50 km depth have a nominal average error smaller than 21 per cent, 27 per cent and 34 per cent, respectively (see figure legends). This finding is valid in extensive interface regions offshore, as illustrated by the ARI distributions and individual checkerboard inversions shown in the first two lines of Supplementary Information Fig. S6. It is important to note that these resolution tests are equally valid for relaxing slip (SSEs) as for back slip (coupling) in their joint inversion.

Figs 4(b) to (e) show the nine-month evolution of aseismic slip in Oaxaca. The slip initiated in a shallow region close to the 2018 (M_w 7.2) Pinotepa earthquake hypocentre, migrated downdip and then along-strike to the east, where the main patch of the O-SSE3 took place in the final two months prior to the earthquake. This event occurred downdip of the 1978 Puerto Escondido earthquake region, between 25 and 55 km depth, and with cumulative moment magnitude M_w 6.6 (M_o = 10.23 x 10^{18} N∗m measured from the slip contour of 0.5 cm and assuming a shear modulus of 32 GPa), which is smaller than the two previous SSEs in Oaxaca (O-SSE1 and O-SSE2) with M_w 6.9 (Table 1). Notably, this SSE occurred in the same region where previous events have been observed (Correa-Mora *et al.* 2008; Graham *et al.* 2016; Cruz-Atienza *et al.* 2021). The SSE clearly did not penetrate the rupture area of the Huatulco earthquake.

Although the transient deformation produced by the SSE is clear from mid-April, the inter-SSE displacement trends in some stations far from the coast started changing well before, around mid-February as shown in Fig. 4(a) (red dashed lines), revealing a gradual plate interface decoupling process at a regional scale preceding the main SSE-induced crustal relaxation (Figs 4b–d and f). Before the decoupling process began (Fig. 4b), the downdip segment of the plate interface, between 25 and 50 km, was fully coupled. Figs 4(d) and (f) further show how the segment downdip of the 1978 earthquake area (dotted circle) is the last one to experience a PIC drop (i.e. the interface slip accelerates but remains below the plate convergence rate) leading to the forthcoming main SSE dislocation patch on April–June, the months preceding the Huatulco

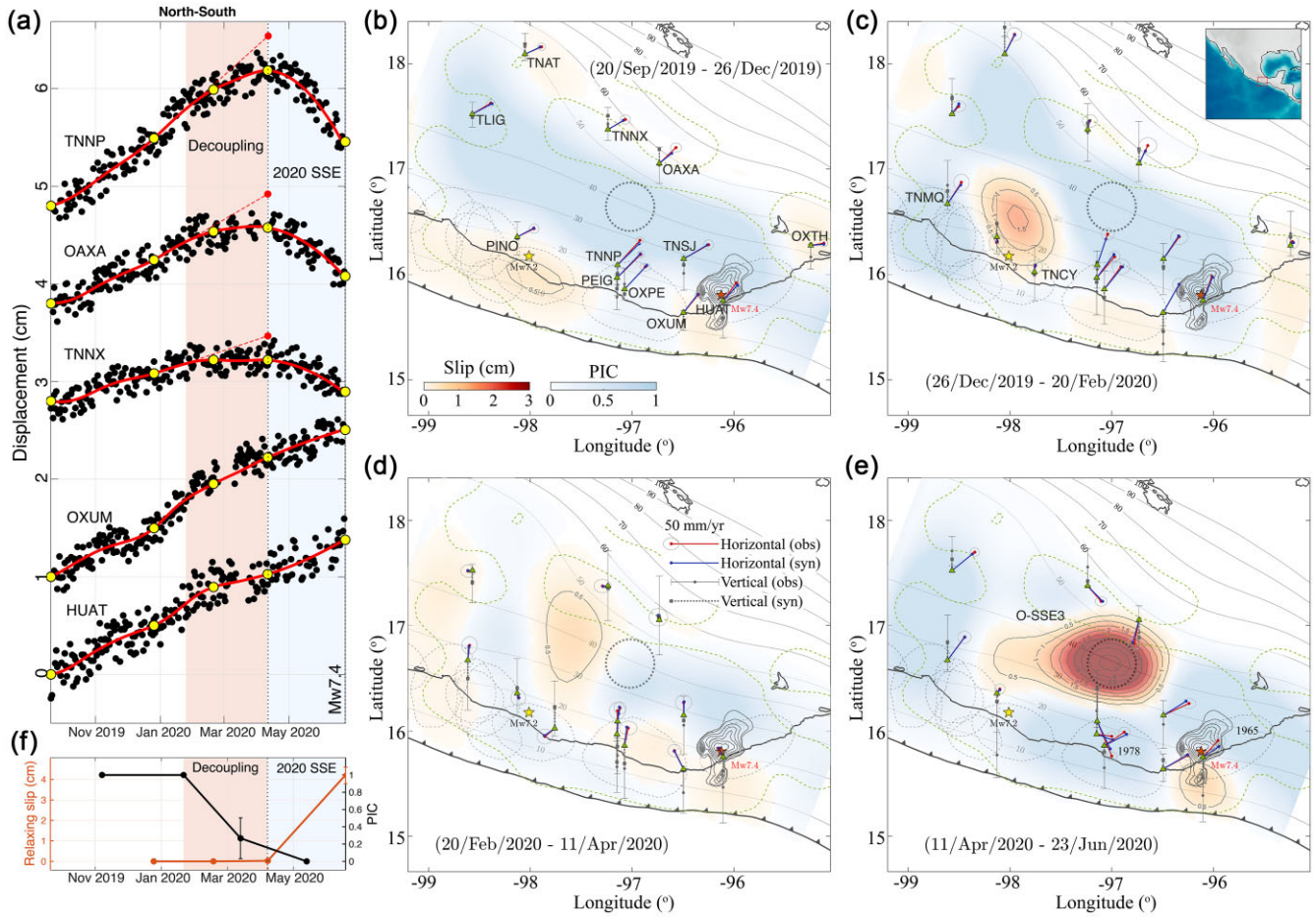

Figure 4. GNSS inversions of the 9-month deformation period prior to the 2020 June 23, M_w 7.4 Huatulco earthquake. (a) North–south GNSS time-series in five selected stations. Yellow dots indicate the beginning and end of the four time-windows used for the slip inversions shown in (b)–(e), solid red line indicates the continuous displacement time-series estimated from the daily GNSS time-series and red dashed lines depict the inter-SSE displacement trend during the interface decoupling phase. (b)–(e) Inverted slip in the plate-convergence (PC) direction for all time windows. Slip contours are in centimetres. Red and yellow stars indicate the epicentres of the Huatulco and 2018 Pinotepa (M_w 7.2) earthquakes, respectively. Dashed regions are the aftershock areas of historic interplate earthquakes. Grey ellipses around the arrow tips represent one standard deviations of the observed displacements. Green dotted lines delineate interface region with slip error smaller than 20 per cent for 100 km patches (see Fig. S6, Supplementary Information). (f) Average and standard deviation (vertical bars) of the plate interface coupling (PIC) and relaxing slip in the region where the 2020 SSE developed (i.e. within the dotted black circle in b–e).

earthquake (Figs 4e and f). The cumulative seismic moment of such event corresponds to M_w 6.6, which is 0.3 units lower than the 2017 (O-SSE1) and 2019 (O-SSE2) SSEs (Table 1). These observations highlight the regional-wide preparatory phase for the 2020 Oaxaca SSE and, possibly, of the main shock.

A common practice to isolate the deformation associated with slow slip transients is to subtract the inter-SSE linear trend from the GNSS time-series. The residual deformation is then assumed to correspond to the strain released by the SSE. When doing this to invert for the slip at the interface, the preparatory phase of the SSE (i.e. the slow decoupling process preceding the SSE relaxation) is mapped and interpreted as aseismic slip resulting in an overall elastic crustal rebound (i.e. a stress drop). However, since this process instead reveals a gradual decrease in the upper crustal stressing rate (red dashed lines in Fig. 4a), this approach leads to a systematic overestimation of the SSE-related surface displacements and, therefore, of the SSE equivalent seismic moment. This has been also pointed out previously by Ochi & Kato (2013) in the Tokai region in Central Japan.

2.3 Early post-seismic deformation

We inverted the early post-seismic GNSS displacements (i.e. the first 4 months following the earthquake discretized in eight 15-d windows, yellow dots in Fig. 5(a) and Supplementary Information Fig. S7b) produced by the main shock using the same parametrization for the ELADIN method as in the previous section, yielding a total scalar moment of 1.084×10^{20} Nm and M_w 7.3, which is close to the M_w 7.2 afterslip of the 2018 Pinotepa earthquake (Table 1). We then assumed that such displacements are only due to the afterslip on the plate interface, which is a reasonable approximation considering that the viscoelastic relaxation after a similar thrust event 260 km west, the 2012 (M_w 7.5) Ometepec earthquake, was negligible in a six month post-seismic period (Graham *et al.* 2014b).

Three main observations arise from the afterslip evolution of the Huatulco earthquake (Figs 5b–e): (1) the largest slip concentrates between 20 and 50 km depth barely reaching the main SSE patch preceding the earthquake (i.e. downdip from the 1978 rupture area) and overlapping the 2017 SSE (Cruz-Atienza *et al.* 2021) (OSSE-1

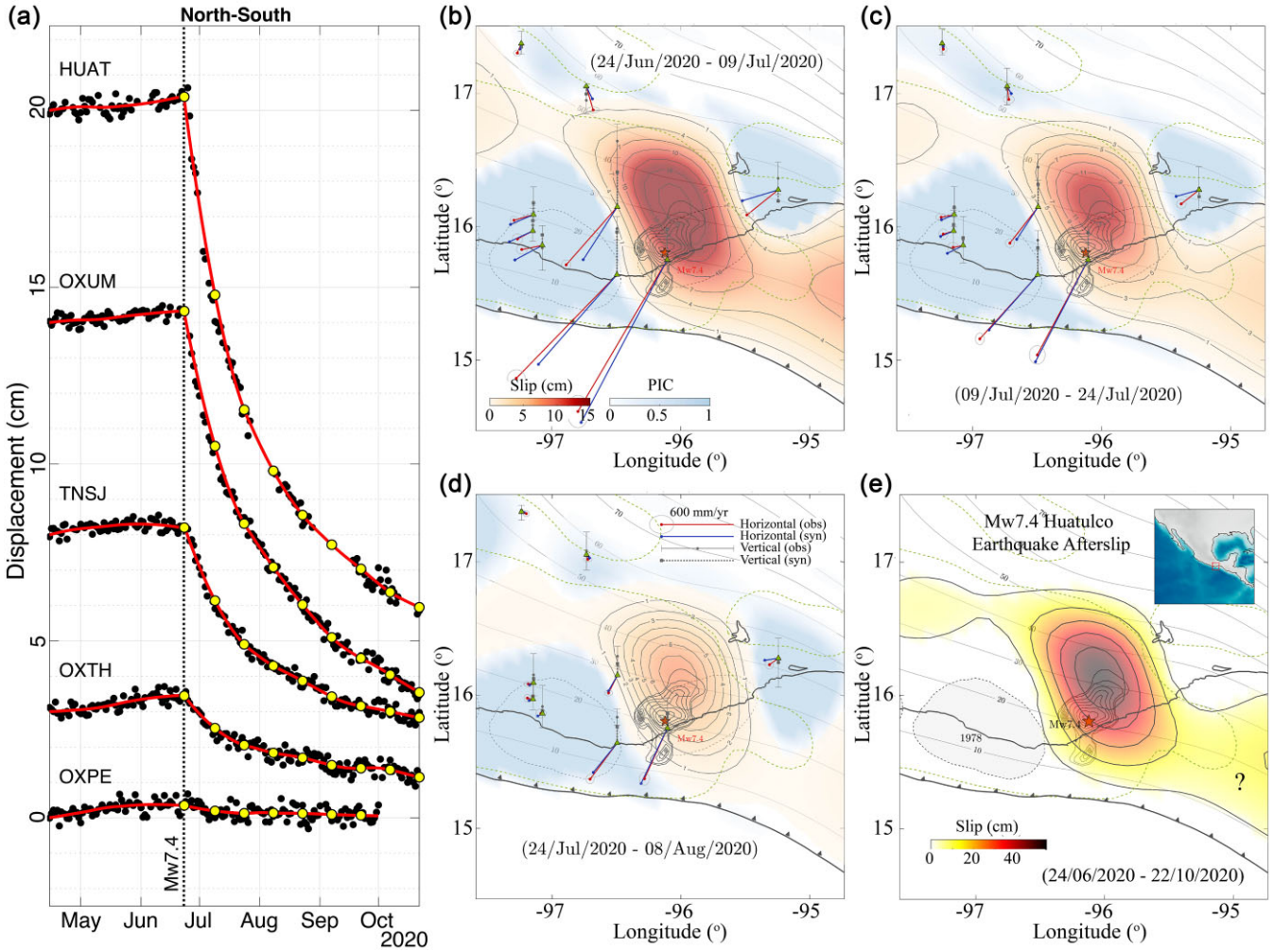

Figure 5. GNSS inversion of the post-seismic deformation of the Huatulco earthquake. (a) North–south displacement GNSS time-series in five selected stations. Yellow dots indicate the start and the end of the six 15-d windows used for the slip inversions, some of them shown in (b–e) (note the dates in every panel). (b–d) Aseismic slip evolution for the post-seismic phase of the Huatulco earthquake. Thick light grey contours are the coseismic slip shown in Fig. 2(a). Green dotted lines delineate interface region with slip error smaller than 20 per cent for 100 km patches (see Fig. S6, Supplementary Information). (e) Cumulative afterslip during the four months following the earthquake.

in Fig. 6a); (2) the main afterslip area completely overlaps with the coseismic rupture area; (3) the afterslip spreads offshore and possibly towards the oceanic trench where aftershocks concentrated (Fig. 1). Regarding the second observation, although the strain pattern can only be explained by such an overlap, due to resolution limits imposed by the chosen problem regularization, we cannot tell for certain whether the afterslip swept the whole coseismic asperity or rather surrounded it. As for the third observation, our confidence in the solution is supported by our model's ability to resolve slip patches of 50 km with a restitution index greater than 0.7 a few kilometres from the oceanic trench (Supplementary Information Fig. S6). Despite not having offshore geodetic stations, the resolution there is surprisingly high (i.e. slip errors below 30 per cent) due to the shallow depth of the interface and because the oceanic trench is located only 40–55 km away from the coast.

The complete overlap of coseismic and post-seismic slip has been observed in the last three interplate thrust earthquakes (M_w 7) in Oaxaca, the 2012 (M_w 7.5) Ometepec (Graham *et al.* 2014b); the 2018 (M_w 7.2) Pinotepa (Cruz-Atienza *et al.* 2021) and the 2020 (M_w 7.4) Huatulco (this study) events, indicating that these seismogenic segments of the plate interface, with depth range between 10 and 30 km, can release elastic strain energy both seismically and aseismically. Seismic patches that can experience post-seismic afterslip have been observed in other subduction zones (Johnson *et al.* 2012) and as well in numerical models (Yabe & Ide 2018). However, the propagation of the Huatulco earthquake afterslip towards the trench is an interesting feature that clearly differs from the 2018 Pinotepa earthquake, whose afterslip stopped under the coast (i.e. at ∼15 km depth and without offshore propagation, see the next section) (Fig. 6a and Supplementary Information Figs S8e–g). This observation suggests significant lateral variations in the geometrical and/or mechanical characteristics along the Oaxaca subduction zone, especially in the shallow, potentially tsunamigenic interface region.

Another noteworthy feature of the post-seismic process in the region is that the Huatulco earthquake post-slip did not penetrate the rupture area of the 1978 Puerto Escondido earthquake (dashed ellipse in Figs 5b–c), which remained fully coupled during the four-month period. Unlike most of the pre-seismic phase, the PIC in the 1978 rupture area remained fully locked after the earthquake (compare Figs 4 and 5) suggesting significant dynamic implications for the accommodation of post-seismic strain in the region.

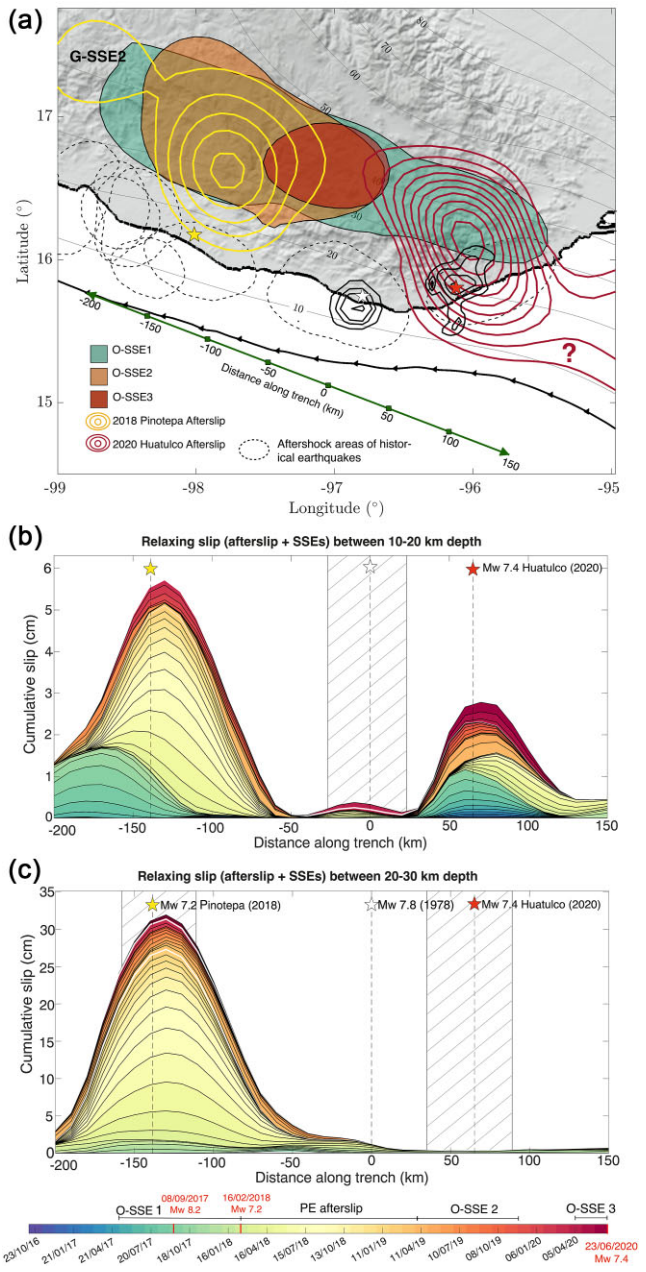

Figure 6. Aseismic slip at the plate interface in Oaxaca. (a) Summary of the aseismic slip processes (SSEs and afterslip) occurring from October 2016 to August 2020 in Oaxaca. Coloured patches indicate the SSEs regions with slip values higher than 2.0 cm. Coloured contours depict the afterslip of the Pinotepa and Huatulco earthquakes with slip isolines every 5 cm beginning with 5 cm. Red, orange and yellow stars indicate the hypocentre of the Huatulco, the 1978 Puerto Escondido and the Pinotepa earthquakes, respectively. Green line indicates the along-trench profile where the evolution of the aseismic slip and CFS on the plate interface is analysed in (b) and (c) and Figs 8 and 9. (b) and (c) show the evolution of the relaxing aseismic slip (SSEs and afterslip) along the trench within the seismogenic zone averaged between 20–30 and 10–20 km depth, respectively. Hatched regions show the interplate segments with the highest moment release of the 2018 Pinotepa, 1978 Puerto Escondido and 2020 Huatulco earthquakes. Stars and dashed black lines indicate the along-trench coordinate of the hypocentres.

3 INTERPLATE SLIP-RATE EVOLUTION IN THE OAXACA SUBDUCTION ZONE

Before the occurrence of the Huatulco earthquake, a complex sequence of SSEs and earthquakes took place in an unusual way along the Mexican subduction zone from April 2017 to September 2019 due to the extremely large, unprecedented seismic waves from the M_w 8.2 Tehuantepec earthquake on 2017 September 8 (Cruz-Atienza *et al.* 2021). During this period, two large SSEs occurred in the downdip interface region of Oaxaca [namely the 2017 SSE (O-SSE1) and the 2019 SSE (O-SSE2)] where the recent 2020 SSE (O-SSE3) took also place (Fig. 6a and Table 1). In fact, the plate interface slipped aseismically and continuously for two years since O-SSE1, experiencing two spontaneous reactivations in this period, one before the Pinotepa earthquake and the other with the O-SSE2 (Cruz-Atienza *et al.* 2021).

We corrected the GNSS displacement time-series used by Cruz-Atienza *et al.* (2021) for seasonal effects from October 2016 to September 2019 as previously done in Section 2.2 (Supplementary Information Fig. S5) and reinverted them for the interplate aseismic slip in detail along the Oaxaca megathrust using the 17 GNSS stations. The new inverted sequence is shown in Supplementary Information Fig. S8. During the sequence, the plate interface experienced remarkable changes of the PIC in the whole megathrust. To analyse the long-term evolution of the aseismic slip before the Huatulco earthquake, we integrated the new corrected slip sequence from October 2016 to September 2019 (Supplementary Information Fig. S8) and the following sequence discussed in Section 2.2 (from September 2019 to June 2020, Fig. 4), and linearly interpolated the complete slip history every 30 d. We also decomposed the total slip into relaxing and stressing interface regions, that is, into SSEs and afterslip regions where the slip rate is greater than the plates convergence rate and, therefore, relax elastic strain (e.g. red gradient zones in Figs 4, 5 and Supplementary Information Fig. S8); and regions under coupling regime, where the velocity of the interplate creep is less than or equal to the plates convergence rate, which increases eastward along the coast (DeMets *et al.* 2010) and, therefore, accumulate elastic strain (e.g. blue gradient zones in Figs 4, 5 and Supplementary Information Fig. S8).

Fig. 6 shows the evolution of the cumulative relaxing slip until the day before the Huatulco earthquake (i.e. projected onto the green line of Fig. 6a) averaged in two different depth ranges, between 10–20 km depth (Fig. 6b) and between 20–30 km depth (Fig. 6c), encompassing the rupture areas of the 2018 Pinotepa, 1978 Puerto Escondido and 2020 Huatulco earthquakes (Fig. 6a). Figs 6(b) and (c) show that the Pinotepa earthquake afterslip (yellow areas) dominates in the region for the analysed period. However, there are other significant slip episodes (i.e. possibly short-term SSEs) often observed in the shallow zone (within the 10–20 km depth range), absent in the 1978 rupture segment, where at least four SSEs offshore Huatulco took place accumulating in 3.5 yr a total slip of 3 cm.

To better examine the interplate slip-rate variations, we averaged the slip at six different locations on the plate interface to analyse its temporal evolution. These locations are denoted by dashed blue circles in the inset maps of Fig. 7 and Supplementary Information Fig. S9, each having a radius of 29 km, to match with the area of our minimum patch size resolution of 50 km. We categorized these locations based on their depth: the first group, DS, corresponds to deeper regions approximately spanning 20–30 km, while the second group, SS, is associated with shallower areas ranging approximately

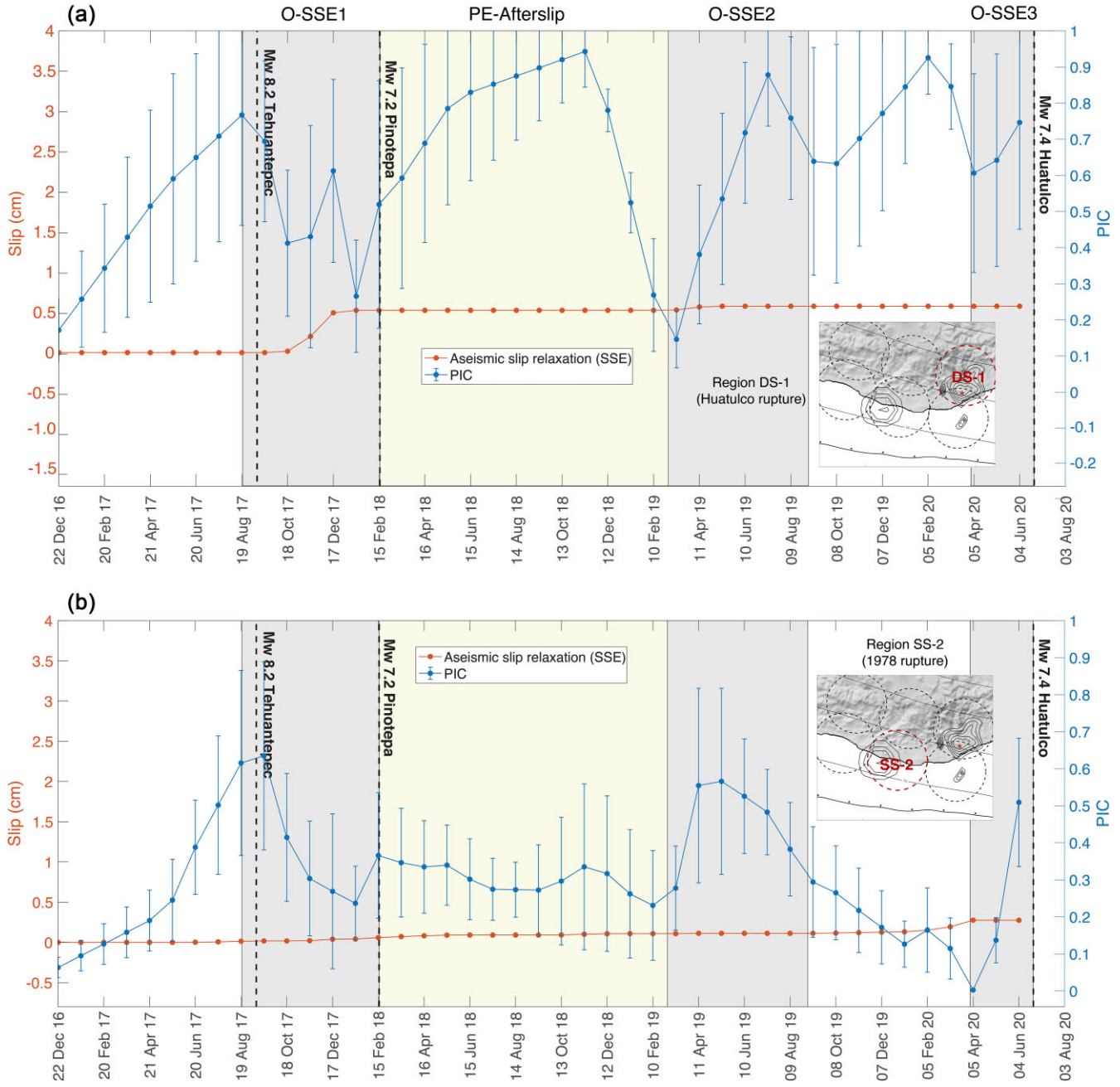

Figure 7. Detailed evolution of the aseismic slip in the seismogenic segment of Oaxaca. Red curves show the relaxing slip (left y-axes) and blue curves the plate interface coupling (PIC, right y-axes) in (a) Region DS-1, the Huatulco rupture area, and (b) Region SS-2, the 1978 Puerto Escondido rupture area. Inset maps show the location of analyzed regions indicated by red dashed circles. Grey rectangles indicate the time windows of the downdip SSEs in Oaxaca. The light-yellow rectangle depicts the timespan of the 2018 Pinotepa earthquake afterslip in the region.

from 10 to 20 km in depth. Region DS-1 is located over the main rupture area of the Huatulco earthquake; Region SS-2, over the rupture area of the 1978 Puerto Escondido earthquake as estimated by Mikumo *et al.* (2002); Region DS-2, downdip from the rupture area of the Puerto Escondido earthquake; Region SS-1, updip from the Huatulco earthquake where most of the aftershocks occurred; and Regions SS-3 and DS-3, west and northwest of the Puerto Escondido earthquake. Fig. 7 and Supplementary Information Fig. S9 show the evolution of the relaxing slip (red line) and the PIC (blue line) within each of the six regions.

The Huatulco rupture area (Fig. 7a; region DS-1) is mainly characterized by PIC variations in the whole analysed period. Slip relaxation took place only during a period of time after the M_w 8.2 Tehuantepec earthquake, when aseismic stress release occurred during the late phase of the O-SSE1 (see Fig. 6a and Supplementary Information Fig. S8c). This phase of the O-SSE1 was indeed triggered by the quasi-static and dynamic stresses produced by the great Tehuantepec event as demonstrated by Cruz-Atienza *et al.* (2021). We also find a gradual four-month decrease of PIC down to 0.1–0.2 at the end of the afterslip period of the

Pinotepa earthquake that eventually recovers during the O-SSE2 to remain high (around 0.8) high until the Huatulco earthquake occurs.

In the 1978 rupture area (Region SS-2, Fig. 7b), there is no significant evidence of aseismic stress release (red line), so that the region slips mostly as creep. In this seismogenic region, PIC changes (blue line) correlate remarkably well with the occurrence of downdip SSEs in Oaxaca (grey rectangles) even though these events did not penetrate the shallow region. During the SSEs, PIC gradually increases to values of 0.5–0.7 in the initial stage of every SSE and then decreases in their final stage to remain relatively low values, down to 0.2–0.4 observed during the inter-SSE periods. This remarkable behaviour, which suggests a non-intuitive interaction between deep SSEs and the coupling regime in the shallower seismogenic zone, is also found in Region SS-3 (Supplementary Information Fig. S9b), west of the 1978 rupture area.

To the east, updip of the Huatulco earthquake (Region SS-1, Supplementary Information Fig. S9a) we find a different and more consistent low PIC value across the whole studied period (between 0 and 0.4) with the exception of a prominent increase after the Tehuantepec earthquake, which might be associated with the stress shadow produced in this specific spot by the great M_w 8.2 rupture (Suárez *et al.* 2019; Cruz-Atienza *et al.* 2021). As pointed out earlier for this region, the red curve indicates that it is likely that small and persistent short-term, episodic SSEs occur in this offshore region over time that can also be appreciated in Figs 4(b)–(e) and 6(b). Such a particular aseismic slip behaviour is consistent with the significant afterslip that swept that shallow area close to the trench after the Huatulco earthquake (Fig. 5). These observations along with the Huatulco earthquake offshore propagation suggest that mechanical properties of this offshore region are prone to release seismically and aseismically the accumulated tractions, as recently found in the western segment of the Guerrero seismic gap (Plata-Martínez *et al.* 2021).

Finally, downdip from the 1978 rupture area (Regions DS-2 and DS-3, Supplementary Information Figs S9c and S9d) we observe a highly variable PIC evolution because of its proximity to the deep SSEs region. During the occurrence of SSEs, PIC reductions begin well before the silent events, meaning that creeping in some subfaults of these regions gradually accelerates before reaching the plates convergence velocity and thus initiating the stress drop (see how the blue curves start decreasing before the red curves start growing in Fig. 7). These observations also indicate that SSEs might partly penetrate these deep seismogenic regions (20–30 km depth) (see also Fig. 6a).

4 IMPLICATIONS OF SSES AND PIC CHANGES ON THE STRESS BUILD-UP

We estimated the CFS changes (Nikkhoo & Walter (2015), see section 4 of the Supplementary Information) produced by the relaxing slip (SSEs and afterslip) and the interplate coupling to elucidate how the stress evolves along the Oaxaca segment (Supplementary Information Fig. S8). For this analysis we have also included the coseismic stress changes produced by the Tehuantepec (Cruz-Atienza *et al.* 2021), Pinotepa (Li *et al.* 2020) and Huatulco earthquakes. Fig. 8 shows the cumulative CFS every 30 d from October 2016 up to the Huatulco event on June 2020 along the trench (i.e. projected onto the green line in Fig. 6a) averaged on two different depth ranges encompassing the main rupture areas of the 2018 Pinotepa and 2020 Huatulco earthquakes (between 20 and 30 km depth, Fig. 8a) and the 1978 Puerto Escondido (between 10 and 20 km depth, Fig. 8b) earthquake. One should bear in mind that these estimates of the CFS are the result of stress contributions from the whole plate interface and not just from the subfaults delimited by the corresponding depth ranges.

For the deeper region (Fig. 8a) the CFS in Huatulco always increased up to values ranging from 60 to 80 kPa. We also observe a CFS contribution of ∼10 kPa induced by the M_w 8.2 Tehuantepec earthquake in the eastern limit of the Huatulco rupture zone that exceeds 30 kPa further to the east. For the shallower region (Fig. 8b), the CFS systematically decreases and remains negative right updip of the Huatulco rupture reaching values of ∼−90 kPa. This negative CFS is associated with both the stress shadows produced by neighbouring coupled segments and the periodic stress release by short-term SSEs in this offshore segment (Fig. 6b).

Supplementary Information Fig. S10 shows both the long-term and inter-SSE time-invariant interplate coupling models estimated by Radiguet *et al.* (2016) (left column) together with their associated CFS change rate (right column). The long-term coupling model represent the resulting deformation trend over a complete number of SSE strain loading–release cycles (Radiguet *et al.*, 2016). The inter-SSE coupling model considers the deformation trend only during periods between consecutive long-term SSEs. Both models produce large stressing rates mainly in the coupled segment of the 1978 earthquake region. However, they also produce large stress shadows in the adjacent, less coupled regions (both along-dip and along-strike) such as in the Pinotepa and Huatulco rupture zones. Although these time-invariant coupling models may lack some observational coverage compared to the present investigation, they share similar features found by Rousset *et al.* (2016) for the inter-SSE regime, which incorporates all available GPS observations in the region (compare Supplementary Information Fig. S10c and fig. 3B of Rousset *et al.* 2016) and with the more recent short-term coupling estimation by Maubant *et al.* (2022).

In contrast, our time-evolving aseismic slip model predicts a different scenario. Fig. 9(a) shows the cumulative CFS at the time of the Huatulco earthquake including contributions of all aseismic slip processes imaged in the megathrust preceding the event from October 2016 to 2020 June 23 (blue areas). A simple inspection reveals large differences in the stress build-up pattern with respect to the time-invariant models (Supplementary Information Fig. S10), especially in both the Huatulco and Pinotepa rupture areas, and east–southeast of the 1978 Puerto Escondido earthquake zone. The bottom four panels of Fig. 9 show the cumulative (trench-perpendicular average) CFS along the trench for the same two depth ranges analysed earlier. The left column shows the cumulative CFS at the time of the Huatulco earthquake, while the right column shows the same quantity plus its coseismic and post-seismic stress increments (see also Fig. 9d).

In the deeper region at the moment and within the rupture area of the Huatulco earthquake (Fig. 9b), the CFS from our time-evolving slip model (blue area) indicates more than double the CFS predicted by the inter-SSE coupling model by Radiguet *et al.* (2016, personal communication) (yellow area), while their long-term coupling model (orange area) predicts even negative CFS values (i.e. no earthquake potential). Downdip of the 1978 rupture area, the CFS predicted by the three models are consistent (values ranging between 20 and 30 kPa), but to the west of this region our model again predicts very different stress concentrations, which are twice the CFS predicted by the inter-SSE coupling model of Radiguet *et al.* When adding the CFS imparted by the Huatulco earthquake and its post-seismic slip shown in Fig. 9(d), our estimate abruptly increases directly downdip of the 1978 rupture area, from about

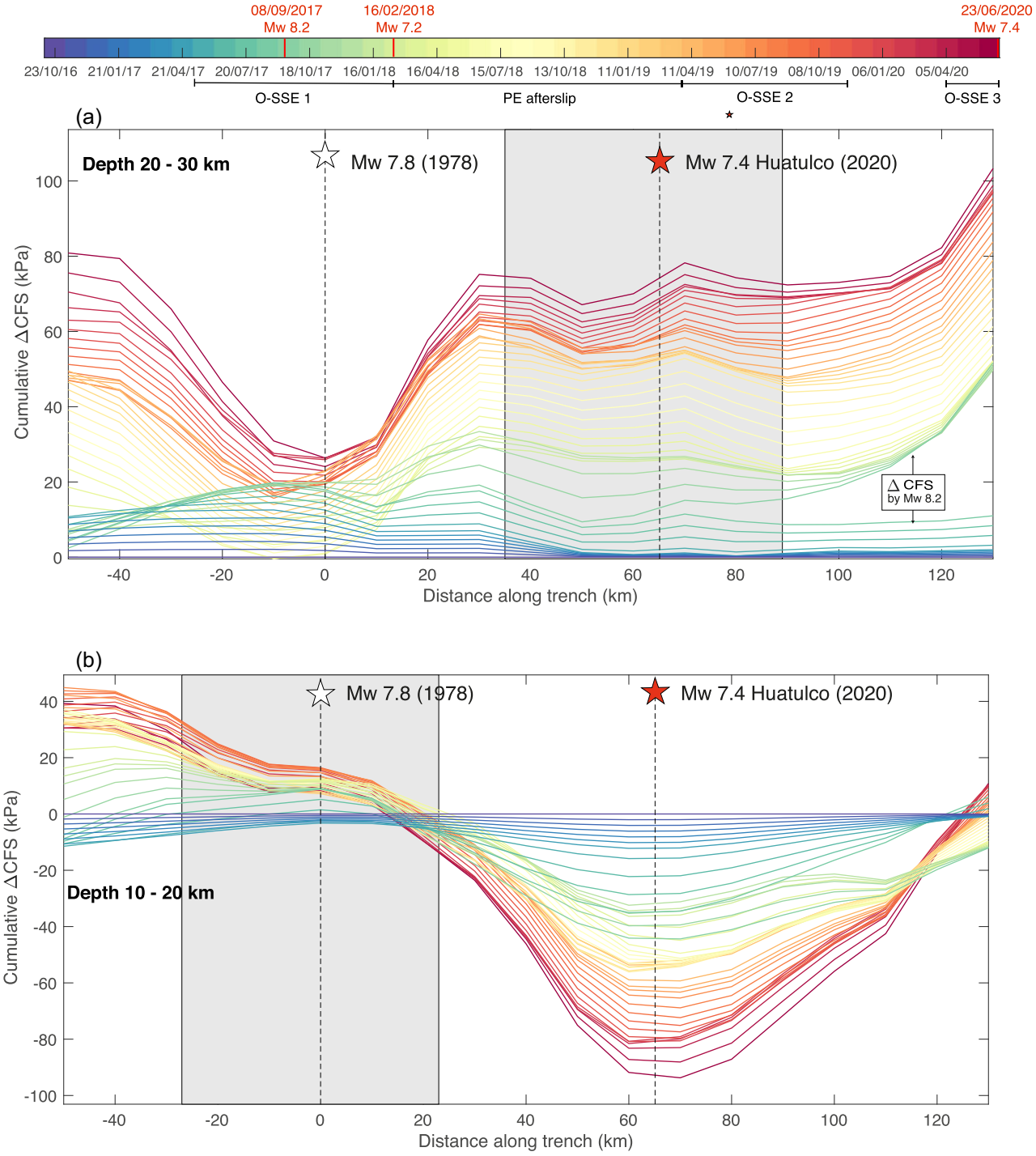

Figure 8. Evolution of the CFS in the seismogenic segment of Oaxaca. Evolution of the total CFS along the trench for every 30 d averaged between (a) 20–30 km and (b) 10–20 km depth. Grey rectangles show the interplate segments with the highest moment release of the 2020 Huatulco earthquake and the 1978 Puerto Escondido event (Mikumo *et al.* 2002).

30 kPa to over 130 kPa. A significant fraction of this value is due to the persistently high coupling in this region throughout the post-seismic phase (Fig. 5). This large, relatively deep segment west of the Huatulco rupture (Region DS-2 in Fig. 6a) might be then highly prone to a future earthquake, as has happened in neighbouring regions over the deep part of the locked zone where the last two interplate earthquakes in Oaxaca (the Pinotepa and Huatulco events) took place, with most of their seismic moment released below 15 km (Fig. 1a and Li *et al.* 2020).

In the shallower region (Fig. 9c), the time-invariant coupling models predict higher CFS values overall than our time-evolving slip model before the Huatulco earthquake, including the 1978 rupture area. Only when adding the coseismic and post-seismic stresses induced by the 2020 earthquake, the inter-SSE model prediction by

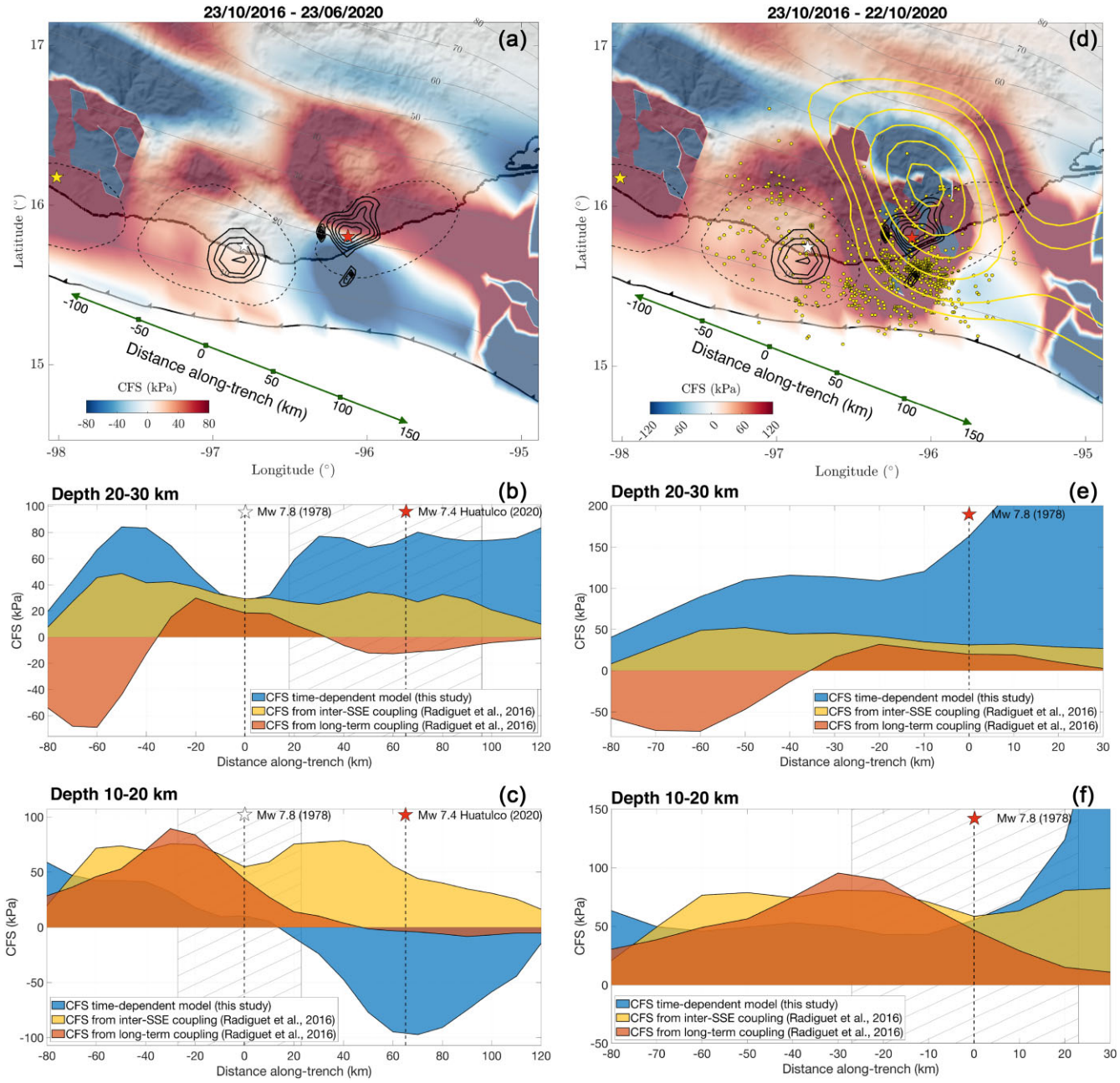

Figure 9. Cumulative CFS from the time-variant model and its comparison with the stress built up predicted by time-invariant coupling models. (a) Cumulative CFS in the plate interface between October 2016 and the date of the 2020 Huatulco earthquake. Black contours represent the isoslip values for the 2020 Huatulco and 1978 Puerto Escondido (Mikumo *et al.* 2002) earthquakes. Black dashed lines delimit the aftershock areas of historic interplate earthquakes. White dashed circles represent the regions where we analyse the evolution of the interplate slip rate and the CFS shown in Figs 6, 7(c) and (d). (b) and (c) Comparison between our cumulative CFS time-variant model and the CFS predicted by time-invariant coupling models of the region between October 2016 and the date of the 2020 Huatulco earthquake for two depth bands, between 20–30 km depth and between 10–20 km depth, respectively. (d) Same than a but including the stress contributions from the coseismic and post-seismic phases of the Huatulco earthquake. Yellow contours are the 5, 10, 20 and 30 cm slip isolines of the two months cumulative afterslip. Yellow dots depict the 50 d aftershocks after the Huatulco Earthquake reported by the SSN. (e) and (f) Same as (b) and (c) but including the stress contribution from the coseismic and post-seismic phases of the Huatulco earthquake focused only in the 1978 rupture segment.

Radiguet *et al.* (2016) becomes similar to ours in the eastern part of the rupture area of the 1978 Puerto Escondido earthquake (Fig. 9f). Only our time-evolving model predicts a large CFS deficit updip of the Huatulco rupture area, which is fully compensated (reaching positive values around 70 kPa) by the coseismic and post-seismic deformations produced by the Huatulco earthquake (Figs 9d and f).

In summary, we can therefore distinguish three major differences between our time-evolving CFS estimates and those from the time-invariant coupling models introduced by Radiguet *et al.* (2016): (1) a high stress concentration over the main downdip rupture area of the Huatulco earthquake before the event predicted only by our model, (2) except for the 1978 rupture segment, absolute CFS values

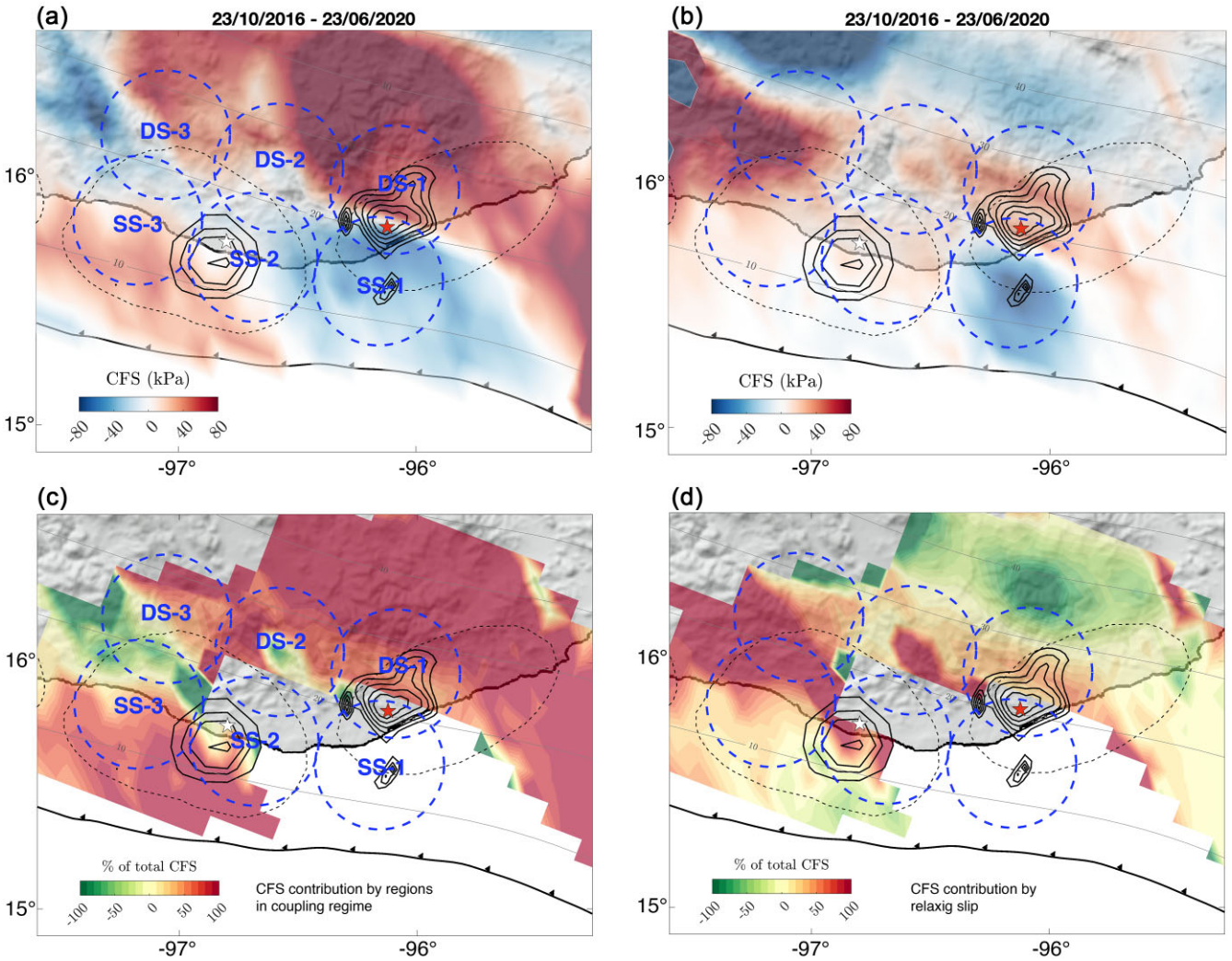

Figure 10. CFS contributions by regions in coupling regime and relaxing slip. (a) and (b) show the cumulative CFS contributions in the plate interface between October 2016 and the date of the 2020 Huatulco earthquake associated with regions in coupling regime and relaxing slip, respectively. (c) and (d) show the CFS contributions (in per cent) on the plate interface where the total CFS is positive (see Fig. 9a) by regions in coupling regime and relaxing slip, respectively. Black contours depict the coseismic slip solution of the 2020 Huatulco event with slip isolines every 0.5 m beginning with 1.0 m.

between 20 and 30 km depth are at least twice as high in our model and (3) a large stress deficit zone updip the Huatulco rupture before the event that is absent in both time-invariant models.

Figs 10(a) and (b) show separately the overall CFS contributions of both the slip under coupling regime and the relaxing slip, respectively, during the whole analysed period before the Huatulco earthquake. Although in different proportions, both stress contributions increase the earthquake potential in the main rupture areas of the Huatulco and 1978 earthquakes. Figs 10(c) and (d) visually depict the percentage ratio of these contributions to the overall CFS (as displayed in Fig. 9a). This analysis is limited to regions displaying positive CFS values, which means to areas with effective seismogenic potential.

Between 20–30 km depth (regions DS-1 and DS-2), we observe that most of the accumulated stress (∼65–80 per cent) was generated by coupled interface regions (Fig. 10c) and the remaining ∼20–35 per cent by the relaxing slip (i.e. long- and short-term SSEs, and the Pinotepa earthquake afterslip) (Fig. 10d) that frequently occurred in the region during more than 3.5 yr (Supplementary Information Figs S11a and S11b). Given its proximity with the Pinotepa earthquake, Region DS-3 differs significantly from this stress partitioning pattern because it is strongly affected by the stresses produced during the coseismic slip and afterslip of the event (Supplementary Information Fig. S11c). The shallower, offshore Region SS-1, which has no pre-stress earthquake potential, experienced a sustained reduction of CFS due to both coupling-related stress shadows (Fig. 10a) and short-term SSEs (Fig. 10b) in similar proportions (Supplementary Information Fig. S11d). This analysis demonstrates the highly heterogeneous stress accumulation and partitioning along the plate interface in the Oaxaca segment.

5 DISCUSSION

Previous M7 class interplate earthquakes in Oaxaca such as those of 1965 and 1928 occurred in close proximity of the 2020 Huatulco rupture, suggesting a possible reactivation of the same asperity over time (Chael & Stewart 1982; Singh *et al.* 1984). Historical data also suggest that two older, probably thrust earthquakes with magnitude larger than 7 occurred nearby in 1870 and 1801 (Suárez

et al. 2020). Assuming that all these events broke the same plate interface segment, their average return period would be 55 ± 13 yr.

In this Oaxaca region, the great M_w ∼8.6 San Sixto earthquake ruptured a ∼300 km along-strike segment in 1787 producing a very large tsunami offshore Oaxaca (Suárez & Albini 2009; Ramírez-Herrera *et al.* 2020). Such event must have involved several locked segments along the Oaxaca megathrust, including shallow portions of the plate interface to generate the mega-tsunami. Whether M8+ events may repeat depends, among other factors, on the interplate mechanical properties and constructive stress interaction between different locked and unlocked fault areas (Kaneko *et al.* 2010, 2018), which evolve with time and may escape from the quantitative analysis of known seismicity over the last century (Nocquet *et al.* 2017). To have an insight into the actual megathrust earthquake potential, that is, to assess whether adjacent locked segments are likely to break jointly to produce a much larger event, it is thus necessary to quantify the stress accumulation through continuous data assimilation as proposed here and in other subduction zones (Saito & Noda 2022, 2023). Monitoring the interplate slip-rate continuously might also allow us to constrain the evolution of frictional parameters that control the fault stability conditions along the complex geometry of the megathrust.

An interesting feature of the Huatulco earthquake is that the rupture mainly propagated downdip, without significant slip in the adjacent updip segment (above ∼15 km depth). Impeding a large rupture into this shallower segment might be partly explained with the existence of the stress barrier produced by both the stress shadow from nearby coupled zones and persistent shallow short-term SSEs (see Figs 6b and 9a). However, other factors such as the geometry of the interface (e.g. subducted plate reliefs in the region, as recently proposed in the Guerrero seismic gap; Plata-Martínez *et al.* 2021) and frictional variations could also contribute to the explanation of this particular rupture pattern. Also interesting is the earthquake initiation at the shallowest extremity of the main asperity and its northward propagation. The nucleation point lies between a highly stressed (downdip) and a highly relaxed (updip) interface regions (Fig. 9a), which means on a place with relatively large stress gradient and, therefore, deformation. The initiation of the earthquake at this point is therefore reasonably explained by our model, as is its main propagation towards the most loaded, downdip interface region.

Our results also suggest that the interplate coupling in Oaxaca is variable in space and time (Fig. 7, Supplementary Information Figs S8 and S9). Such remarkable PIC variations might certainly be related with changes in the mechanical properties of the fault zone materials induced by the dynamic perturbations of seismic waves from recent significant regional earthquakes (Delorey *et al.* 2015; Materna *et al.* 2019; Cruz-Atienza *et al.* 2021). Particularly interesting are the PIC variations in the shallow, seismogenic zone (i.e. between 10 and 20 km depth), which seems to be somehow linked to the occurrence of deeper, long-term SSEs (Fig. 7b and Supplementary Information Fig. S9b). To explain these PIC variations at shallow depths we favour the idea involving transient fluctuations of fluid pressure at the interface, as proposed for the long-term SSEs in the Guerrero (Cruz-Atienza *et al.* 2018), southern Cascadia (Materna *et al.* 2019), Japan (Bedford *et al.* 2020) and Hikurangi (Warren-Smith *et al.* 2019) subduction zones. Recent models evoking the fault-valving concept show that overpressure fluid pulses migrate along the subduction channel as the permeability evolves in the fault zone due to slow deformation processes (Cruz-Atienza *et al.* 2018; Shapiro *et al.* 2018; Zhu *et al.* 2020; Farge *et al.* 2021). These transient changes in pore pressure may lead to large variations of the fault strength as high as ∼10–20 MPa (Zhu *et al.* 2020), which makes this mechanism a plausible candidate to explain the strong and systematic PIC variations we found in the shallow seismogenic zone of Oaxaca during the occurrence of SSEs downdip.

Variations in interplate coupling, similar to those observed in Oaxaca, have been documented in several subduction zones and are often linked to both seismic and aseismic processes. In south-central Alaska, long-term coupling variations have been associated with multiyear slow-slip events (Li *et al.* 2016). In the Hikurangi subduction zone in New Zealand, it has been demonstrated that coupling changes are closely related to the stage of the slow-slip cycle, highlighting the complex dynamics of stress accumulation and release (Maubant *et al.* 2023). Similarly, coupling changes driven by the static and dynamic effects of earthquakes have been identified in Chile (Melnick *et al.* 2017; Hoffmann *et al.* 2018) and southern Cascadia (Materna *et al.* 2019).

Earthquake potential depends on the state of stress along the subduction zone which, as shown here, is a function of different evolving processes taking place from the trench to its deep portion. The stress build-up therefore changes over time and space in a complex way, so does the earthquake potential. Time-invariant estimates of the interplate coupling are often used to identify seismogenic segments prone to large earthquakes (Chlieh *et al.* 2008; Moreno *et al.* 2010; Perfettini *et al.* 2010; Loveless & Meade 2011). However, while these estimates are certainly useful on a large spatial and temporal scale, they do not allow a reliable picture of the earthquake potential associated with smaller ($7 < M < 8.5$) but potentially devastating ruptures that occur more frequently, as shown in this work for the Oaxaca megathrust.

Our results indicate that continuous and systematic monitoring of the interplate slip velocity, incorporating simultaneously the stressing (i.e. coupled) and relaxing (i.e. slow, coseismic and post-seismic) slip regimes in a continuum, provides a more reliable reconstruction of the short-term stress evolution over the megathrust and, probably also, of the long-term evolution which, together with a seismic monitoring of tectonic tremor and repeating earthquakes (Dominguez *et al.* 2022), could provide significant insights into the M8+ earthquake supercycles. Proceeding this way may thus be relevant to evaluate theoretical predictions of the interface dynamics, which is our leading approach to understand the underlying physics in subduction systems.

6 CONCLUSIONS

We analysed the interplate slip-rate evolution during more than 3.5 yr in the Oaxaca subduction zone including the pre-seismic, coseismic and post-seismic phases associated with the 2020 June 23 M_w 7.4 Huatulco earthquake to better understand how the different slip regimes contribute to the plate-interface stress accumulation and thus to the seismogenic potential. We found that the rupture area of the Huatulco earthquake extends between 7 and 33 km depth with a main, compact slip patch around 15 to 25 km depth north–northeast from the hypocentre and a second, much smaller shallow patch offshore and south from the hypocentre where most of aftershocks where located. The entire rupture zone falls within the aftershock area of the 1965 M_s 7.2 earthquake, suggesting rupture of the same or a very close asperity. The long-term, M_w 6.6 SSE that occurred downdip before the earthquake did not penetrate the rupture area and was preceded by a gradual interface decoupling process at a regional scale, including the maximum SSE slip area. During the two months preceding the earthquake, when the strongest phase of the 2020 SSE developed downdip, the Huatulco earthquake

rupture area became fully locked. Our slip inversions indicate that the four-month earthquake afterslip overlapped the whole coseismic rupture area and propagated both to the trench, where most of aftershocks happened, and downdip to the north, where the 2020 SSE was developing. During the post-seismic phase, the rupture area of the 1978 Puerto Escondido earthquake became and remained fully coupled.

The interplate slip-rate evolution in Oaxaca during the 3.5 yr preceding the Huatulco earthquake shows that PIC in the megathrust seismogenic region is highly variable in time and space. One interesting feature of such variations is the correlation between transient PIC increments at shallow depths (10–20 km, including the 1978 rupture area) and the occurrence of three successive SSEs far downdip. This might suggest a physical interaction likely related to fluid diffusion at the interface induced by aseismic slip processes in nearby regions that simultaneously relax and load different interface sections. The implication of this finding is so important that it will be necessary to assess its generality in other regions of Mexico and the world through long-term, continuous spatiotemporal analysis of the slip-rate and the stresses at the plate interface, complemented by further examination of the activity of both regular and slow earthquakes. We also found that both relaxing aseismic slip events and megathrust coupling changes during those 3.5 yr produced a significant stress concentration (∼80 kPa) downdip from the Huatulco earthquake nucleation zone likely promoting the main rupture patch in that segment. Furthermore, these stress contributions produced as well a large and shallow (offshore) stress reduction (∼−90 kPa) that may have impeded (along with other possible factors) a much larger updip propagation of the earthquake with tsunamigenic potential.

Our results indicate that continuous monitoring of the interplate aseismic slip-rate and its CFS counterpart provide a better estimation of M7+ earthquake potential over seismogenic regions than predictions yielded by time-independent interplate coupling models. Analysis of the stress partition in the Oaxaca region indicates that downdip SSEs can contribute up to 35 per cent of the accumulated stress in the seismogenic zone. Finally, the stress imparted during the coseismic and post-seismic phases of the Huatulco earthquake on the 1978 Puerto Escondido rupture area (and its downdip portion between 20 and 30 km depth) makes it a region prone to another earthquake in the near future, a forecast consistent with the ∼55 yr return period in this Oaxaca region.

ACKNOWLEDGMENTS

We are grateful for the outstanding technical support of Eduardo Murrieta and Luciano Díaz in the maintenance of the Gaia supercomputing platform, and Luis Salazar in the TLALOCNet field operations and stations maintenance. We thank Mathilde Radiguet for kindly providing us the long-term coupling models. We also thank Shri Krishna Singh, Arturo Iglesias and Gerardo Suárez for fruitful discussion; the Servicio Sismológico Nacional (SSN), the Servicio Mareográfico Nacional (SMN) and the Servicio de Geodesia Satelital, all of them from the Instituto de Geofísica-UNAM, for all GNSS, strong motion and tide gauge data, as well as all their personnel for data acquisition and distribution; and the European Space Agency for access to the Sentinel1 data. This work is partially based on GNSS data belonging also to TLALOCNet and services provided by the NSF GAGE Facility, operated by EarthScope Consortium, with support from the National Science Foundation, the National Aeronautics and Space Administration and the U.S. Geological Survey under NSF Cooperative Agreement EAR-1724794. All GNSS data have been processed in the Laboratorio de Geodesia Satelital (LaGeos) of the Instituto de Geofísica-UNAM. This work was supported by CONACyT grants 6471 and 255308, UNAM-PAPIIT grants IN113814, IG100617 and IG100921 and IN111524, JICA-JST SATREPS-UNAM grant 15543611, UNAM-DGTIC grant LANCAD-312 and the graduate school scholarships by CONACyT. CV was supported by the European Research Council grant PERSISMO (grant 865411).

AUTHOR CONTRIBUTIONS

C. Villafuerte (Conceptualization, Formal analysis, Investigation, Methodology, Visualization, Writing – original draft), V. M. Cruz-Atienza (Conceptualization, Investigation, Methodology, Project administration, Resources, Supervision, Visualization, Writing – review and editing), J. Tago (Investigation, Methodology, Software, Validation, Writing – review and editing), D. Solano-Rojas (Data curation, Investigation, Validation, Writing – review and editing), R. Garza-Girón (Data curation, Formal analysis, Investigation, Methodology, Writing – review and editing), S. I. Franco (Data curation, Writing – review and editing), L. A. Dominguez (Investigation, Writing – review and editing), and V. Kostoglodov (Investigation, Resources, Writing – review and editing)

SUPPORTING INFORMATION

Supplementary data are available at *GJIRAS* online.

Figure S1. Vertical (Z), east–west (EW) and north–south (NS) coseismic displacements estimated from the GNSS time-series at stations HUAT, OXUM, TNSJ, OXTH, OXPE, TNNP and OAX2.

Figure S2. Huatulco earthquake coseismic displacements estimated from the HUAT tide gauge

Figure S3. Coseismic slip inversions for the Huatulco earthquake using different data sets. Coseismic slip inversion (upper panel) and their associated misfit GNSS and LOS displacements errors (lower panels) using (a) both GNSS and InSAR data, (b) only GNSS data and (c) only InSAR data.

Figure S4. GNSS displacement time-series estimated with the Gipsy-Oasis (v6.4) software for the pre-seismic period in the 12 stations and the three components. GNSS time-series partially belong to TLALOCNet network and the services provided by the NSF GAGE Facility (Cabral-Cano *et al.* 2015a; Cabral-Cano *et al.* 2015b, Cabral-Cano *et al.* 2016; Cabral-Cano *et al.* 2016b; Demets and Cabral-Cano 2008; UNAVCO Community, 2014a; UNAVCO Community 2014b; UNAVCO Community 2016a; UNAVCO Community 2016b).

Figure S5. Example of the correction of displacement time-series in station TNSJ, TNNP and TNNX and TLIG for seasonal effects. Left column: Pre-processed GNSS time-series (black dots) and seasonal functions for every component (red curves) estimated from the multiwindow fit procedure. Light blue rectangles indicate the period of the OSSEs. Right column: Original (red dots) and corrected (blue dots) displacement time series. The dashed black lines in both columns indicate the occurrence of the 2017Tehuantepec Earthquake, the 2018 Pinotepa earthquake and the 2020 Huatulco Earthquake.

Figure S6. Resolution analysis for aseismic slip inversions in Oaxaca. Each column presents the analysis considering slip patch sizes of a 100 km, b 70 km and c 50 km. First row: Example of a target checkerboard test for each slip patch size. Cyan circles are

GNSS stations. Black dashed lines indicate isodepths of the plate interface. Second row: Inverted checkerboard results. Third row: Average restitution index obtained from the mobile checkerboard inversion. Green dashed lines indicate isodepths of the plate interface. Green circles represent the GNSS stations. Note that the shallow plate interface regions are well-resolved in all cases, owing to their proximity to the trench along the coast.

Figure S7. East–west and vertical GNSS displacement time-series estimated with the Gipsy-Oasis software for the pre-seismic (a) and post-seismic; (b) periods in selected stations shown in Figs 4 and 5.

Figure S8. Left column: Evolution of aseismic slip inversions in Oaxaca from October 2016 to September 2019, including the 2017 Oaxaca slow slip event (O-SSE1), afterslip from the Pinotepa earthquake (PE-afterslip) and the 2019 Oaxaca slow slip event (O-SSE2). Right column: Cumulative coulomb failure stress (CFS) on the plate interface, considering both relaxing slip and changes in plate interface coupling, calculated since the beginning of the sequence up to the time indicated by the second date in the left column's title. The CFS contributions from the 2018 M_w 7.2 Pinotepa earthquake and the 2017 M_w 8.2 Tehuantepec earthquake are also included.

Figure S9. Evolution of the relaxing aseismic slip (red curves, SSEs and afterslip) and plate interface coupling (blue curves, PIC) in regions a SS-1, b DS-2, c SS-3 and d DS-3. Right column indicates the location of each region.

Figure S10. Long-term and inter-SSE time-invariant interplate coupling models estimated by Radiguet *et al.* (2016, personal communication) for the Oaxaca subduction zone and their associated CFS rates.

Figure S11. Evolution of the stress partitioning in the seismogenic zone in Oaxaca. Every panel show the evolution of the total CFS (black curves) and their contributions from the relaxing aseismic slip (red curve) and coupled regions (yellow curve), for Regions DS-(1-3) and SS- (1-3). Grey rectangles indicate the occurrence of SSEs in the region. The light-yellow rectangle shows the period when the post-seismic afterslip of the 2018 Pinotepa and 2020 Huatulco earthquakes developed in the region. Continuous and dashed green lines depict the CFS contribution estimated by the long-term and inter-SSE coupling models, respectively.

Please note: Oxford University Press is not responsible for the content or functionality of any supporting materials supplied by the authors. Any queries (other than missing material) should be directed to the corresponding author for the paper.

CONFLICT OF INTEREST

The authors have no competing or conflict of interest in what is expressed in this paper.

DATA AVAILABILITY

Part of the GPS data analysed in this study are available under some restrictions in the repository of the 'Servicio Sismológico Nacional de la UNAM' (http://www.ssn.unam.mx). Broad-band seismic data are publicly available in the same repository. Part of the GPS data in the state of Oaxaca are available in the repository of the 'TLALOCNet del Instituto de Geofísica de la UNAM' (http://tlalocnet.udg.mx). The rest of the GPS data in the state of Guerrero are not publicly available until March 2026 due to the restriction policies of the SATREPS-UNAM research project. For more information contact the corresponding author.

CODE AVAILABILITY

Custom computer programs and mathematical algorithms that are deemed central to the conclusions of this study are available on request from the corresponding author.

REFERENCES

Amiri-Simkooei, A.R., Tiberius, C.C. & Teunissen, P.J., 2007. Assessment of noise in GPS coordinate time series: methodology and results, *J. geophys. Res.: Solid Earth,* **112**(B7).

Bedford, J.R., Moreno, M., Deng, Z., Oncken, O., Schurr, B., John, T., Báez, J.C. & Bevis, M., 2020. Months-long thousand-kilometre-scale wobbling before great subduction earthquakes, *Nature,* **580**(7805), 628–635.

Beroza, G.C. & Ide, S., 2011. Slow earthquakes and nonvolcanic tremor, *Annu. Rev. Earth planet. Sci.,* **39,** 271–296.

Cabral-Cano, E. *et al.*, 2018. TLALOCNet: a continuous GPS-Met backbone in Mexico for seismotectonic and atmospheric research, *Seism. Res. Lett.,* **89**(2A), 373–381.

Chael, E.P. & Stewart, G.S., 1982. Recent large earthquakes along the Middle American trench and their implications for the subduction process, *J. geophys. Res.: Solid Earth,* **87**(B1), 329–338.

Chlieh, M., Avouac, J.-P., Sieh, K., Natawidjaja, D.H. & Galetzka, J., 2008. Heterogeneous coupling of the Sumatran megathrust constrained by geodetic and paleogeodetic measurements, *J. geophys. Res.: Solid Earth,* **113**(B5).

Correa-Mora, F., DeMets, C., Cabral-Cano, E., Marquez-Azua, B. & Diaz-Molina, O., 2008. Interplate coupling and transient slip along the subduction interface beneath Oaxaca, Mexico, *Geophys. J. Int.,* **175**(1), 269–290.

Cotte, N., Walpersdorf, A., Kostoglodov, V., Vergnolle, M., Santiago, J.-A. & Campillo, M., 2009. Anticipating the next large silent earthquake in Mexico, *Eos, Trans. Am. Geophys. Un.,* **90**(21), 181–182.

Cruz-Atienza, V.M. *et al.*, 2021. Short-term interaction between silent and devastating earthquakes in Mexico, *Nat. Commun.,* **12**(1), 2171.

Cruz-Atienza, V.M., Villafuerte, C. & Bhat, H.S., 2018. Rapid tremor migration and pore-pressure waves in subduction zones, *Nat. Commun.,* **9**(1), 1–13.

Delorey, A.A., Chao, K., Obara, K. & Johnson, P.A., 2015. Cascading elastic perturbation in Japan due to the 2012 M_w 8.6 Indian Ocean earthquake, *Sci. Adv.,* **1**(9), e1500468.

DeMets, C., Gordon, R.G. & Argus, D.F., 2010. Geologically current plate motions, *Geophys. J. Int.,* **181**(1), 1–80.

Dominguez, L., Taira, T., Cruz-Atienza, V., Iglesias, A., Villafuerte, C., Legrand, D., Pérez-Campos, X. & Raggi, M., 2022. Interplate slip rate variation between closely spaced earthquakes in southern Mexico: the 2012 Ometepec and 2018 Pinotepa Nacional thrust events, *J. geophys. Res.: Solid Earth,* **127**(6), e2022JB024292.

Farge, G., Jaupart, C. & Shapiro, N.M., 2021. Episodicity and migration of low frequency earthquakes modeled with fast fluid pressure transients in the permeable subduction interface, *J. geophys. Res.: Solid Earth,* **126**(9), e2021JB021894.

Graham, S. *et al.*, 2016. Slow slip history for the Mexico subduction zone: 2005 through 2011, in *Geodynamics of the Latin American Pacific, Margin W. L. Bandy, J. Dañobeitia, C. Gutiérrez, Y. Taran, R. Bartolomé, Eds.,* pp. 3445–3465, Springer International Publishing, 2017.

Graham, S.E. *et al.*, 2014a. GPS constraints on the 2011–2012 Oaxaca slow slip event that preceded the 2012 March 20 Ometepec earthquake, southern Mexico, *Geophys. J. Int.,* **197**(3), 1593–1607.

Graham, S.E. *et al.*, 2014b. GPS constraints on the M_w= 7.5 Ometepec earthquake sequence, southern Mexico: coseismic and post-seismic deformation, *Geophys. J. Int.,* **199**(1), 200–218.

Guo, R., Yang, H., Zhu, Y., Zheng, Y., Xu, J., Zhang, L. & An, C., 2021. Narrow rupture of the 2020 M_w 7.4 La Crucecita, Mexico, Earthquake, *Seism. Soc. Am.,* **92**(3), 1891–1899. https://doi.org/10.1785/0220200328.

Heki, K. & Mitsui, Y., 2013. Accelerated pacific plate subduction following interplate thrust earthquakes at the Japan trench, *Earth planet. Sci. Lett.,* **363,** 44–49.

Hoffmann, F., Metzger, S., Moreno, M., Deng, Z., Sippl, C., Ortega-Culaciati, F. & Oncken, O., 2018. Characterizing afterslip and ground displacement rate increase following the 2014 Iquique-Pisagua M_w 8.1 earthquake, northern Chile, *J. geophys. Res.: Solid Earth,* **123**(5), 4171–4192.

Ito, Y. *et al.*, 2013. Episodic slow slip events in the Japan subduction zone before the 2011 Tohoku-Oki earthquake, *Tectonophysics,* **600,** 14–26.

Johnson, K.M., Fukuda, J. & Segall, P., 2012. Challenging the rate-state asperity model: afterslip following the 2011 M9 Tohoku-oki, Japan, earthquake, *Geophys. Res. Lett.,* **39**(20).

Kaneko, Y., Avouac, J.-P. & Lapusta, N., 2010. Towards inferring earthquake patterns from geodetic observations of interseismic coupling, *Nat. Geosci.,* **3**(5), 363–369.

Kaneko, Y., Wallace, L.M., Hamling, I.J. & Gerstenberger, M.C., 2018. Simple physical model for the probability of a subduction-zone earthquake following slow slip events and earthquakes: application to the Hikurangi megathrust, New Zealand, *Geophys. Res. Lett.,* **45**(9), 3932–3941.

Kato, A., Obara, K., Igarashi, T., Tsuruoka, H., Nakagawa, S. & Hirata, N., 2012. Propagation of slow slip leading up to the 2011 M_w 9.0 Tohoku-Oki earthquake, *Science,* **335**(6069), 705–708.

Lay, T. & Kanamori, H., 1981. An asperity model of large earthquake sequences, in *Earthquake Prediction,* eds Simpson, D. W. & Richards, P. G., Wiley. doi: 10.1029/ME004p0579.

Li, S., Freymueller, J. & McCaffrey, R., 2016. Slow slip events and time-dependent variations in locking beneath lower cook inlet of the Alaska-Aleutian subduction zone, *J. geophys. Res.: Solid Earth,* **121**(2), 1060–1079.

Li, Y., Shan, X., Zhu, C., Qiao, X., Zhao, L. & Qu, C., 2020. Geodetic model of the 2018 M_w 7.2 Pinotepa, Mexico, earthquake inferred from InSAR and GPS data, *Bull. seism. Soc. Am.,* **110**(3), 1115–1124.

Loveless, J.P. & Meade, B.J., 2011. Spatial correlation of interseismic coupling and coseismic rupture extent of the 2011 M_w= 9.0 Tohoku-oki earthquake, *Geophys. Res. Lett.,* **38**(17).

Materna, K., Bartlow, N., Wech, A., Williams, C. & Bürgmann, R., 2019. Dynamically triggered changes of plate interface coupling in Southern Cascadia, *Geophys. Res. Lett.,* **46**(22), 12 890–12 899.

Maubant, L., Frank, W.B., Wallace, L.M., Williams, C.A. & Hamling, I., 2023. Imaging the spatiotemporal evolution of plate coupling with interferometric radar (InSAR) in the Hikurangi subduction zone, *Geophys. Res. Lett.,* **50**(19), e2023GL105388.

Maubant, L., Radiguet, M., Pathier, E., Doin, M.-P., Cotte, N., Kazachkina, E. & Kostoglodov, V., 2022. Interseismic coupling along the Mexican subduction zone seen by InSAR and GNSS, *Earth planet. Sci. Lett.,* **586,** 117534.

Melgar, D., Pérez-Campos, X., Ramirez-Guzman, L., Spica, Z., Espíndola, V.H., Hammond, W.C. & Cabral-Cano, E., 2018. Bend faulting at the edge of a flat slab: The 2017 Mw7. 1 Puebla-Morelos, Mexico earthquake, *Geophys. Res. Lett.,* **45**(6), 2633–2641.

Melgar, D., Ruiz-Angulo, A., Pérez-Campos, X., Crowell, B.W., Xu, X., Cabral-Cano, E., Brudzinski, M.R. & Rodriguez-Abreu, L., 2021. Energetic rupture and tsunamigenesis during the 2020 M_w 7.4 La Crucecita, Mexico Earthquake, *Seism. Soc. Am.,* **92**(1), 140–150. doi: 10.1785/0220200272.

Melnick, D., Moreno, M., Quinteros, J., Baez, J.C., Deng, Z., Li, S. & Oncken, O., 2017. The super-interseismic phase of the megathrust earthquake cycle in Chile, *Geophys. Res. Lett.,* **44**(2), 784–791.

Mikumo, T., Yagi, Y., Singh, S.K. & Santoyo, M.A., 2002. Coseismic and postseismic stress changes in a subducting plate: possible stress interactions between large interplate thrust and intraplate normal-faulting earthquakes, *J. geophys. Res.: Solid Earth,* **107**(B1), ESE–5.

Mirwald, A., Cruz-Atienza, V.M., Díaz-Mojica, J., Iglesias, A., Singh, S.K., Villafuerte, C. & Tago, J., 2019. The 19 September 2017 (M_w 7.1) intermediate-depth Mexican earthquake: a slow and energetically inefficient deadly shock, *Geophys. Res. Lett.,* **46**(4), 2054–2064.

Moreno, M., Rosenau, M. & Oncken, O., 2010. 2010 Maule earthquake slip correlates with pre-seismic locking of Andean subduction zone, *Nature,* **467**(7312), 198–202.

Nikkhoo, M. & Walter, T.R., 2015. Triangular dislocation: an analytical, artefact-free solution, *Geophys. J. Int.,* **201**(2), 1119–1141.

Nocquet, J.-M. *et al.*, 2017. Supercycle at the Ecuadorian subduction zone revealed after the 2016 Pedernales earthquake, *Nat. Geosci.,* **10**(2), 145–149.

Obara, K. & Kato, A., 2016. Connecting slow earthquakes to huge earthquakes, *Science,* **353**(6296), 253–257.

Ochi, T. & Kato, T., 2013. Depth extent of the long-term slow slip event in the Tokai district, central Japan: a new insight, *J. geophys. Res.: Solid Earth,* **118**(9), 4847–4860.

Perfettini, H. *et al.*, 2010. Seismic and aseismic slip on the Central Peru megathrust, *Nature,* **465**(7294), 78–81.

Plata-Martínez, R. *et al.*, 2021. Shallow slow earthquakes to decipher future catastrophic earthquakes in the Guerrero seismic gap, *Nat. Commun.,* **12,** 3976. doi:

Radiguet, M. *et al.*, 2016. Triggering of the 2014 M_w 7.3 Papanoa earthquake by a slow slip event in Guerrero, Mexico, *Nat. Geosci.,* **9**(11), 829–833.

Ramírez-Herrera, M.-T. *et al.*, 2020. Sand deposits reveal great earthquakes and tsunamis at Mexican Pacific Coast, *Sci. Rep.,* **10**(1), 1–10.

Rousset, B. *et al.*, 2016. Lateral variations of interplate coupling along the Mexican subduction interface: relationships with long-term morphology and fault zone mechanical properties, *Pure appl. Geophys.,* **173**(10), 3467–3486.

Saffer, D.M. & Wallace, L.M., 2015. The frictional, hydrologic, metamorphic and thermal habitat of shallow slow earthquakes, *Nat. Geosci.,* **8,** 594–600.

Saito, T. & Noda, A., 2022. Mechanically coupled areas on the plate interface in the Nankai Trough, Japan and a possible seismic and aseismic rupture scenario for megathrust earthquakes, *J. geophys. Res.: Solid Earth,* **127**(8), e2022JB023992.

Saito, T. & Noda, A., 2023. Mechanically coupled areas on the plate interface in the Kanto region, Central Japan, generating great earthquakes and slow-slip events, *Bull. seism. Soc. Am.,* **113**(5), 1842–1855.

Savage, J.C., Svarc, J.L. & Yu, S.-B., 2005. Postseismic relaxation and transient creep, *J. geophys. Res.: Solid Earth,* **110**(B11).

Segall, P. & Bradley, A.M., 2012. Slow-slip evolves into megathrust earthquakes in 2D numerical simulations, *Geophys. Res. Lett.,* **39**(18).

Shapiro, N.M., Campillo, M., Kaminski, E., Vilotte, J.-P. & Jaupart, C., 2018. Low-frequency earthquakes and pore pressure transients in subduction zones, *Geophys. Res. Lett.,* **45**(20), 11–083.

Singh, S., Astiz, L. & Havskov, J., 1981. Seismic gaps and recurrence periods of large earthquakes along the Mexican subduction zone: a reexamination, *Bull. seism. Soc. Am.,* **71**(3), 827–843.

Singh, S., Dominguez, T., Castro, R. & Rodriguez, M., 1984. *P* waveform of large, shallow earthquakes along the Mexican subduction zone, *Bull. seism. Soc. Am.,* **74**(6), 2135–2156.

Singh, S., Reinoso, E., Arroyo, D., Ordaz, M., Cruz-Atienza, V., Pérez-Campos, X., Iglesias, A. & Hjörleifsdóttir, V., 2018. Deadly intraslab Mexico earthquake of 19 September 2017 (M_w 7.1): ground motion and damage pattern in Mexico City, *Seism. Res. Lett.,* **89**(6), 2193–2203.

Socquet, A. *et al.*, 2017. An 8 month slow slip event triggers progressive nucleation of the 2014 Chile megathrust, *Geophys. Res. Lett.,* **44**(9), 4046–4053.

Suárez, G. & Albini, P., 2009. Evidence for great tsunamigenic earthquakes (*M* 8.6) along the Mexican subduction zone, *Bull. seism. Soc. Am.,* **99**(2A), 892–896.

Suárez, G., Ruiz-Barón, D., Chico-Hernández, C. & Zúñiga, F.R., 2020. Catalog of preinstrumental earthquakes in central Mexico: epicentral and magnitude estimations based on macroseismic data, *Bull. seism. Soc. Am.,* **110**(6), 3021–3036.

Suárez, G., Santoyo, M.A., Hjorleifsdottir, V., Iglesias, A., Villafuerte, C. & Cruz-Atienza, V.M., 2019. Large scale lithospheric detachment of the downgoing Cocos plate: the 8 September 2017 earthquake (M_w 8.2), *Earth planet. Sci. Lett.,* **509,** 9–14. doi: 10.1016/j.epsl.2018.12.018.

Tago, J., Cruz-Atienza, V.M., Villafuerte, C., Nishimura, T., Kostoglodov, V., Real, J. & Ito, Y., 2021. Adjoint slip inversion under a constrained

optimization framework: revisiting the 2006 Guerrero slow slip event, *Geophys. J. Int.,* **226**(2), 1187–1205.

Uchida, N., Iinuma, T., Nadeau, R.M., Bürgmann, R. & Hino, R., 2016. Periodic slow slip triggers megathrust zone earthquakes in northeastern Japan, *Science,* **351**(6272), 488–492.

UNAM-Seismology-Group, 2013. Ometepec-Pinotepa Nacional, Mexico earthquake of 20 March 2012 (M_W 7.5): a preliminary report, *Geof. Int.,* **52**(2), 173–196.

Voss, N., Dixon, T.H., Liu, Z., Malservisi, R., Protti, M. & Schwartz, S., 2018. Do slow slip events trigger large and great megathrust earthquakes?, *Sci. Adv.,* **4**(10), eaat8472.

Warren-Smith, E. *et al.*, 2019. Episodic stress and fluid pressure cycling in subducting oceanic crust during slow slip, *Nat. Geosci.,* **12**(6), 475–481.

Wen, Y., Xiao, Z., He, P., Zang, J., Liu, Y. & Xu, C., 2021. Source characteristics of the 2020 M_w 7.4 Oaxaca, Mexico, earthquake estimated from GPS, InSAR, and teleseismic waveforms, *Seism. Soc. Am.,* **92**(3), 1900–1912.

Xie, Z., Cai, Y., Wang, C.-y., Yoshioka, S. & Tanaka, M., 2019. Fault stress inversion reveals seismogenic asperity of the 2011 M_w 9.0 Tohoku-oki Earthquake, **9**(1), 11987. doi: 10.1038/s41598-019-47992-x.

Yabe, S. & Ide, S., 2018. Why do aftershocks occur within the rupture area of a large earthquake?, *Geophys. Res. Lett.,* **45**(10), 4780–4787.

Yan, Z., Xiong, X., Liu, C. & Xu, J., 2022. Integrated analysis of the 2020 M_w 7.4 La Crucecita, Oaxaca, Mexico, Earthquake from joint inversion of geodetic and seismic observations, *Bull. seism. Soc. Am.,* **112**(3), 1271–1283.

Zhu, W., Allison, K.L., Dunham, E.M. & Yang, Y., 2020. Fault valving and pore pressure evolution in simulations of earthquake sequences and aseismic slip, *Nat. Commun.,* **11**(1), 1–11.